Study of MSSM heavy Higgs bosons decaying into charginos and neutralinos

Rahool Kumar Barman,[1,*] Biplob Bhattacherjee,[1,†] Amit Chakraborty,[2,‡] and Arghya Choudhury[3,4,§]

[1]*Centre for High Energy Physics, Indian Institute of Science, Bangalore 560012, India*
[2]*Department of Theoretical Physics, Tata Institute of Fundamental Research, 1, Homi Bhabha Road, Mumbai 400005, India*
[3]*Consortium for Fundamental Physics, Department of Physics and Astronomy, University of Sheffield, Sheffield S3 7RH, United Kingdom*
[4]*Consortium for Fundamental Physics, Department of Physics and Astronomy, University of Manchester, Manchester M13 9PL, United Kingdom*

(Received 22 July 2016; published 21 October 2016)

A multitude of searches have already been performed by the ATLAS and CMS collaborations at the LHC to probe the heavy Higgses of the minimal supersymmetric Standard Model (MSSM) through their decay to the Standard Model particles. In this paper, we study the decay of the MSSM heavy Higgses into neutralino and chargino pairs and estimate the maximum possible branching ratios for these "ino" modes being consistent with the present LHC data. After performing a random scan of the relevant electroweakino parameters, we impose the SM 125 GeV Higgs constraints and low-energy flavor data. We choose a few representative benchmark points satisfying all the above-mentioned constraints as well as the current bounds on heavy Higgses and electroweakinos from the LHC Run-I and Run-II data. We then perform a detailed collider simulation, including fast detector effects, and analyze all the potential SM backgrounds in order to estimate the discovery reach of these heavy Higgses at the LHC. We restrict ourselves within the leptonic cascade decay modes of these heavy Higgses and study the mono-$\mathrm{X} + \not{E}_T$ ($\mathrm{X} = W, Z$) and trilepton $+ \not{E}_T$ signatures in the context of a high-luminosity run of the 14 TeV LHC.

DOI: 10.1103/PhysRevD.94.075013

I. INTRODUCTION

The observation of a resonance around 125 GeV by the ATLAS and CMS collaborations has led to a new era in particle physics [1,2]. Comprehensive studies to investigate the spin and parity quantum numbers of the observed particle prefer its scalar nature. Various properties of this newly discovered resonance also seem to be in good accordance with that of the Standard Model (SM) Higgs boson. However, it is to be noted that even though large deviations from the SM predictions have already been excluded from the current LHC data, nonstandard Higgs couplings are still allowed within the present uncertainties in various Higgs coupling measurements [3–5]. Thus, the possibility of the observed resonance being a part of an extended Higgs sector is not ruled out by the current LHC data; what we require is very precise measurement of various couplings of the observed Higgs boson to the SM particles.

Supersymmetry (SUSY) [6–8] has been so far one of the most popular frameworks for formulating physics beyond the SM (BSM); however, a SUSY signature is yet to be observed at the LHC [9,10]. The Higgs sector of the minimal supersymmetric Standard Model (MSSM) is phenomenologically richer compared to that of the SM [7,8]. The model has two CP-even neutral Higgses (the lighter and heavier ones are h and H, respectively), one CP-odd neutral Higgs (A), and two charged scalars ($H^{\pm}$). At the tree level, the Higgs sector of the MSSM can be parametrized by two parameters: $\tan\beta$, the ratio of the vacuum expectation value of the two Higgs doublets ($H_{u,d}$), and the pseudoscalar Higgs mass M_A. In the MSSM, the lightest CP-even Higgs boson has a mass which lies below M_Z at the tree level. To reconcile the observed Higgs mass at 125 GeV, one needs to invoke large higher-order loop corrections involving the SM and SUSY particles. Soon after the Higgs discovery, numerous studies were performed to look for additional Higgs-like states by both the ATLAS and CMS collaborations at the LHC. For example, both the ATLAS and CMS collaborations have studied the decay of the CP-even heavy scalar boson (H) into a pair of photons [11,12], W bosons [13,14], Z bosons [15], and SM-like 125 GeV Higgs bosons (h) [16–20] through various possible final-state topologies. The decay of the CP-odd pseudoscalar Higgs boson (A) into a h and Z boson has also been studied with $\sqrt{s} = 8$ TeV data by both LHC collaborations [21,22]. Moreover, the decay of the neutral Higgs bosons H/A to a pair of tau leptons has also been studied by the ATLAS and CMS collaboration using $\sqrt{s} = 7$ and $\sqrt{s} = 8$ TeV data [23,24]. This search mode

*rahoolkbarman@chep.iisc.ernet.in
†biplob@chep.iisc.ernet.in
‡amit@theory.tifr.res.in
§a.choudhury@sheffield.ac.uk

has been found to be by far one of the most efficient channels to constrain the MSSM parameter space. For example, using the $H/A \to \tau^+\tau^-$ channel, regions with large $\tan\beta$ (say > 20) and small M_A (say < 500 GeV) are already excluded by the LHC Run-II data. Comprehensive studies have also been performed to search for the charged Higgs bosons. The CMS Collaboration has looked for the charged Higgses via its decay to $\tau^+\nu_\tau$, $c\bar{s}$ and $t\bar{b}$, when H^+ is produced from the $t\bar{t}$ and/or $pp \to \bar{t}(b)H^+$ processes [25–27]. Studies of H^+ decaying to a tau lepton and a neutrino have been performed by the ATLAS Collaboration using the data set collected at $\sqrt{s} = 8$ TeV corresponding to an integrated luminosity of 19.5 fb^{-1} [28,29]. The ATLAS Collaboration has searched for charged Higgs in the $c\bar{s}$ decay channel as well using $\sqrt{s} = 7$ TeV data [30]. All of the above-mentioned studies have not been able to find any compelling signature of the heavy Higgs bosons, and hence 95% C.L. upper limits on the production cross section times the branching ratios have been placed for a wide range of MSSM heavy resonance masses.

From the above discussions it is clear that all of the aforementioned LHC analyses of the MSSM neutral and charged Higgs bosons rely on their decay to the SM particles. However, we have to keep in mind that the decay of these heavy MSSM Higgses to light supersymmetric particles, if kinematically allowed, would modify the branching ratios of the heavy Higgses to SM particles considerably. Let us consider an example: a CP-even heavy Higgs H can decay, if kinematically allowed, to a pair of neutralinos which then decays to a SM Higgs and/or Z and the lightest neutralino, with h/Z decaying through their usual decay modes. A few sample processes are shown below:

$$H, A \to \tilde{\chi}_2^0 + \tilde{\chi}_1^0, \qquad \tilde{\chi}_2^0 \to h/Z + \tilde{\chi}_1^0,$$
$$H, A \to \tilde{\chi}_2^0 + \tilde{\chi}_3^0, \qquad \tilde{\chi}_2^0 \to h/Z + \tilde{\chi}_1^0,$$
$$\tilde{\chi}_3^0 \to h/Z + \tilde{\chi}_2^0.$$

Many such processes are possible, when these decays are kinematically allowed, and most of these decays lead to a wide range of final-state topologies which can be tested at the LHC. The study of this very interesting possibility is the key motivation of this paper. One can ask the following set of questions: (a) what are the relative branching ratios of the heavy Higgses decaying into the electroweakinos (i.e., charginos and neutralinos)? (b) how large/small can these heavy Higgs decay modes be, while still satisfying the LHC Run-I and Run-II Higgs data?; (c) do the Run-II and future high-luminosity runs of the LHC have the sensitivity to search for these heavy resonances through these electroweakino channels? In this paper, we attempt to answer these questions by performing a parameter-space scan satisfying current LHC data and then analyzing the decay of the MSSM heavy Higgses to electroweakinos through mono-X plus missing energy (X $= W, Z$) and the trilepton plus missing energy signatures with a detailed collider study. Here we restrict ourselves within these mono-X and trilepton searches as these analyses are simpler and also well understood in the context of the LHC. Moreover, note that the branching ratios of the neutralinos/charginos to W, Z involved final states are quite large and thus we expect to have better sensitivity through these modes. Earlier phenomenological studies on the decay of H and A to a pair of charginos and neutralinos can be seen in Refs. [31–44]. One-loop effects on these decay modes have also been estimated [45–47]. From the experimental front, preliminary studies by the ATLAS and CMS collaborations have shown that the regions of the parameter space with heavy Higgs masses around 200–500 GeV decaying to neutralinos/charginos can be probed with $100/300\ \mathrm{fb}^{-1}$ of luminosity at the 14 TeV run of the LHC [48,49]. The plan of this paper can be summarized as follows.

(i) We first demand that the properties of the lightest Higgs boson (h) are consistent with those of the observed 125 GeV Higgs boson satisfying all the present constraints from the 7 and 8 TeV LHC data. We restrict ourselves within R-parity-conserving SUSY where the lightest supersymmetric particle (LSP), here the lightest neutralino $\tilde{\chi}_1^0$, is stable and constitutes a source of missing transverse energy ($\not{E}_T$).

(ii) We then perform a random scan of the relevant MSSM parameters and then satisfy the updated 125 GeV Higgs data and low-energy flavor data. After discussing salient features of the parameter space allowed by the above two constraints, we choose a few representative benchmark points satisfying the current LHC bounds on the heavy Higgses as well as electroweakinos.

(iii) Finally, we perform dedicated collider studies for the heavy Higgses associated to the selected benchmark points through mono-X ($X = W, Z$) plus missing energy as well as trilepton plus missing energy ($\not{E}_T$) signatures in the context of a 14 TeV high-luminosity run of the LHC.

The rest of this paper is organized in the following order. We discuss the coupling of the MSSM Higgs bosons h, H, A, and $H^\pm$ to electroweakino pairs in Sec. II A. In Secs. II B and II C we discuss the various constraints used in our analysis, followed by the details of the parameter-space scan. Existing collider bounds on the heavy Higgses and electroweakino masses are discussed in Sec. II D, followed by a discussion on some representative benchmark points in Sec. III A. The collider phenomenology focusing on the mono-X + $\mathrm{E}_\mathrm{T}^\mathrm{miss}$ ($X = W/Z$) and trilepton + $\not{E}_T$ states arising from the decay of the heavy Higgses to electroweakinos are discussed in Secs. III B and III C. Finally, we summarize our results in Sec. IV.

II. AVAILABLE PARAMETER SPACE AND LHC DATA

A. Higgs couplings to electroweakinos

The decay of the MSSM heavy Higgs bosons to electroweakinos, namely charginos and neutralinos, crucially depends on the chargino/neutralino mixing matrices. The decay width of a generic Higgs boson H_k (with $k = 1, 2, 3, 4$ representing the h, H, A, and $H^\pm$ Higgses, respectively) to a pair of neutralinos ($\tilde{\chi}_1^0$, $\tilde{\chi}_2^0$, $\tilde{\chi}_3^0$, $\tilde{\chi}_4^0$) and charginos ($\tilde{\chi}_1{}^\pm$, $\tilde{\chi}_2{}^\pm$) can be written as [8]

$$\Gamma(H_k \to \tilde{\chi}_i \tilde{\chi}_j) \sim M_{H_k}\left[((g^L_{ijk})^2 + (g^R_{ijk})^2)\left(1 - \frac{m^2_{\tilde{\chi}_i}}{M^2_{H_k}} - \frac{m^2_{\tilde{\chi}_j}}{M^2_{H_k}}\right) - 4\epsilon_i\epsilon_j g^L_{ijk} g^R_{ijk}\frac{m_{\tilde{\chi}_i} m_{\tilde{\chi}_j}}{M^2_{H_k}}\right], \tag{1}$$

where $\epsilon_i = \pm 1$ denotes the sign of the ith eigenvalue of the neutralino mass matrix, while $\epsilon_i = 1$ is the same for charginos with $\tilde{\chi}_i, \tilde{\chi}_j$ representing generic electroweakinos. The left- and right-handed couplings associated to the neutral Higgs bosons ($H_\ell = h$, H, A, respectively, with $\ell = 1, 2, 3$) with the neutralinos and charginos can be written as [8]

$$g^L_{\tilde{\chi}_i{}^0 \tilde{\chi}_j{}^0 H_\ell} = \frac{1}{2s_w}(N_{j2} - \tan\theta_w N_{j1})(e_\ell N_{i3} + d_\ell N_{i4}) + i \leftrightarrow j, \tag{2}$$

$$g^R_{\tilde{\chi}_i{}^0 \tilde{\chi}_j{}^0 H_\ell} = \frac{1}{2s_w}(N_{j2} - \tan\theta_w N_{j1})(e_\ell N_{i3} + d_\ell N_{i4})\epsilon_\ell + i \leftrightarrow j, \tag{3}$$

$$g^L_{\tilde{\chi}_i{}^+ \tilde{\chi}_j{}^- H_\ell} = \frac{1}{\sqrt{2}s_w}(e_\ell V_{j1} U_{i2} - d_\ell V_{j2} U_{i1}), \tag{4}$$

$$g^R_{\tilde{\chi}_i{}^+ \tilde{\chi}_j{}^- H_\ell} = \frac{1}{\sqrt{2}s_w}(e_\ell V_{i1} U_{j2} - d_\ell V_{i2} U_{j1})\epsilon_\ell, \tag{5}$$

while the same couplings for the charged Higgs bosons are given by

$$g^L_{\tilde{\chi}_i{}^\pm \tilde{\chi}_j{}^0 H^\mp} = \frac{\cos\beta}{s_w}\left[N_{j4} V_{i1} + \frac{1}{\sqrt{2}}(N_{j2} + \tan\theta_w N_{j1}) V_{i2}\right], \tag{6}$$

$$g^R_{\tilde{\chi}_i{}^\pm \tilde{\chi}_j{}^0 H^\mp} = \frac{\sin\beta}{s_w}\left[N_{j3} U_{i1} + \frac{1}{\sqrt{2}}(N_{j2} + \tan\theta_w N_{j1}) U_{i2}\right]. \tag{7}$$

The coefficients e_ℓ and d_ℓ have the following definitions:

$$e_1 = \cos\alpha, \qquad e_2 = -\sin\alpha, \qquad e_3 = \sin\beta,$$
$$d_1 = -\sin\alpha, \qquad d_2 = \cos\alpha, \qquad d_3 = \cos\beta,$$

and $\epsilon_{1,2} = 1$, $\epsilon_3 = -1$, where $s_w = \sin\theta_w$ (θ_w being the Weinberg angle), α is the Higgs mixing angle, and $\tan\beta$ is the ratio of the vacuum expectation value of the MSSM two-Higgs doublets. The 2×2 matrices U and V diagonalize the chargino mass matrix, while the 4×4 matrix N denotes the diagonalizing matrix for the neutralinos.

From the above-mentioned equations (2)–(7), one can observe that the couplings of the MSSM Higgses with the electroweakinos crucially depend on their compositions. It is evident that the Higgses will couple with the neutralinos and charginos if and only if there exists an admixture of the Higgsinos and gauginos in the electroweakino mass eigenstates. The coupling of the Higgs bosons with "ino" pairs would be highly suppressed if both of the inos are either Higgsino dominated or gaugino dominated. Now, for example, let us consider the limit $M_1 < M_2 \ll \mu$. From the neutralino mass matrix we observe that the lightest mass eigenstate $\tilde{\chi}_1^0$ will be bino dominated and $\tilde{\chi}_2^0$ will be wino dominated, while $\tilde{\chi}_3^0$ and $\tilde{\chi}_4^0$ are Higgsino dominated. In this context, the decay modes $H \to \tilde{\chi}_1^0\tilde{\chi}_2^0, \tilde{\chi}_3^0\tilde{\chi}_4^0, \tilde{\chi}_1^+\tilde{\chi}_1^-, \tilde{\chi}_2^+\tilde{\chi}_2^-$ will be suppressed, and the dominant "ino" modes will be those which are manifestly mixtures of gaugino and Higgsinos, like $H \to \tilde{\chi}_1^0\tilde{\chi}_3^0, \tilde{\chi}_2^0\tilde{\chi}_3^0, \tilde{\chi}_1^+\tilde{\chi}_2^-$, etc. Depending on the choice of the electroweakino mass parameters, a wide range of possibilities can arise which may lead to interesting phenomenological collider signatures.

In order to obtain a clear picture of the above-mentioned scenario, in Fig. 1 we show the branching fractions of the heavy Higgses H (upper left), A (upper right), and $H^\pm$ (lower) decaying to SM particles as well as modes involving electroweakinos. To generate the particle spectrum we use SUSPECT (version 2.43) [50] while HDECAY (version 6.41) [51] is used to calculate the branching fractions of the heavy Higgses. Here we vary $\tan\beta$ from 5 to 55 with the following choices:

$$\begin{aligned} &M_A = 650\ \text{GeV}, \qquad M_1 = 500\ \text{GeV}, \\ &M_2 = 150\ \text{GeV}, \qquad \mu = 300\ \text{GeV}, \\ &M_3 = 5\ \text{TeV}, \qquad m_{\tilde{Q}_{3l}} = m_{\tilde{t}_R} = m_{\tilde{b}_R} = 5\ \text{TeV}, \\ &A_t = -5\ \text{TeV}, \qquad A_b = A_\tau = 0. \end{aligned} \tag{8}$$

From Fig. 1 it is evident that we find regions[1] with relatively smaller values of $\tan\beta$ where the non-SM decay

[1]In this simple-minded scan, we do not impose the updated Higgs constraints or any low-energy physics constraints, except for the fact the lightest Higgs boson should have a mass between 122–128 GeV. In a more dedicated scan, as we discuss in the next section, we do consider all these constraints.

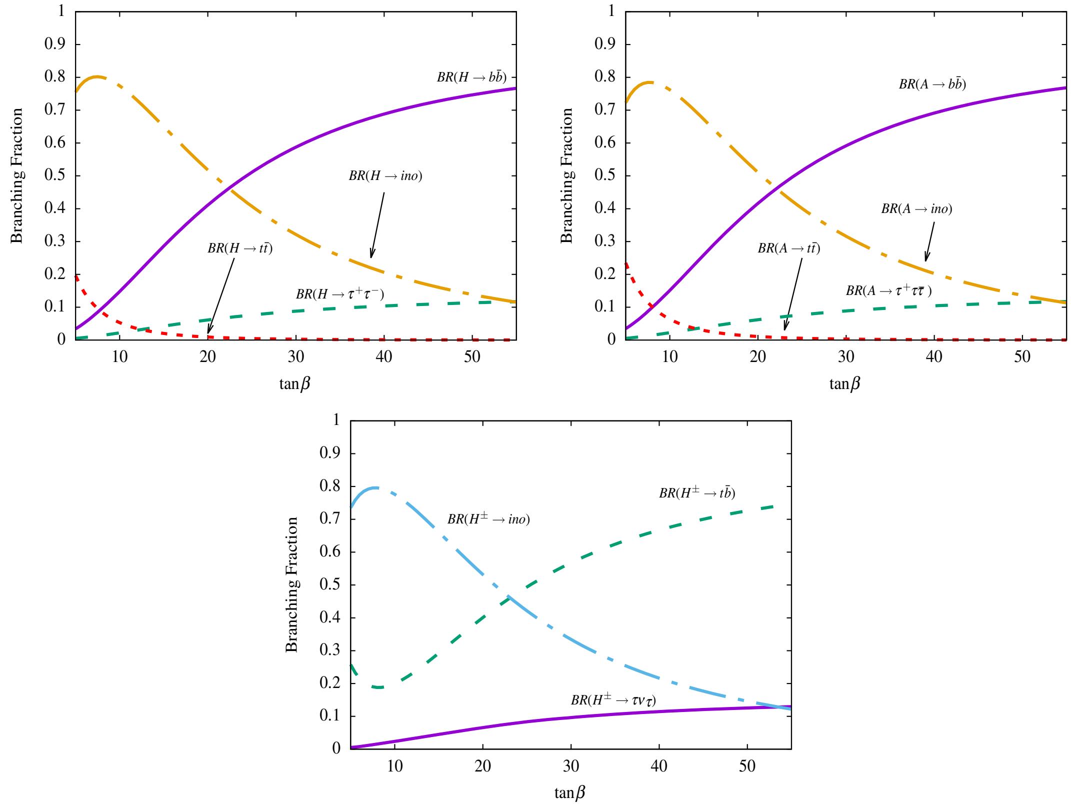

FIG. 1. The variation of the heavy Higgs (H, A, $H^{\pm}$) branching fractions with $\tan\beta$ for both the SM and non-SM "ino" decay modes. Here the term "ino" refers to the combined chargino and neutralino decay modes of the respective heavy Higgs bosons.

modes (i.e., "ino" modes) gain dominance over the SM ones. The non-SM branching ratio is calculated by summing all possible "ino" decay modes of the Higgs boson; for example, for H they are $H \to \tilde{\chi}_i^0\tilde{\chi}_j^0$ (i, $j = 1-4$) and $H \to \tilde{\chi}_i{}^+\tilde{\chi}_j{}^-$ (i, $j = 1-2$) modes. Note that, in the low-$\tan\beta$ region, the $H \to t\bar{t}$ channel is enhanced because of the $\cot\beta$ proportionality factor in the $Ht\bar{t}$ coupling. The $H \to b\bar{b}$ channel dominates in the high-$\tan\beta$ region because of the $Hb\bar{b}$ coupling which is directly proportional to $\tan\beta$. The behavior of the $H \to \tau^+\tau^-$ channel is also the same as the $b\bar{b}$ mode. As a result of these dominant SM branching ratios, the decays of the neutral and charged heavy Higgses to neutralino and/or chargino pairs are suppressed at very low and very high $\tan\beta$ regions. We find that, in order to obtain appreciable branching ratios (at least 10% or more) to the non-SM "ino" modes, we are required to focus on the regions with moderate values of $\tan\beta$, say, the $\tan\beta = 5-20$ regime.

Before we end this section, we would like to briefly discuss how the individual "ino" modes behave with the variation of $\tan\beta$. In Fig. 2, we display the dominant "ino" decay modes of the heavy Higgs bosons H (upper panel) and A (lower panel). The individual "ino" modes of the charged Higgs boson are shown in Fig. 3. From both Figs. 2 and 3, it is evident that the dominant $\phi \to$ ino ($\phi = H$, A, $H^{\pm}$) decay modes are those which are compounded from Higgsino and gaugino mixing. For example, the H, $A \to \tilde{\chi}_1^+\tilde{\chi}_1^-$ decay mode is highly suppressed as compared to the H, $A \to \tilde{\chi}_1^+\tilde{\chi}_2^-$ decay mode due to small gaugino-Higgsino mixing. Similarly, in the case of $H, A \to \tilde{\chi}_i^0\tilde{\chi}_j^0$ (i, $j = 1-4$) decay modes, those channels in which both the neutralinos are either Higgsino dominated or gaugino dominated are suppressed as compared to the ones where the neutralinos are manifestly mixed states of gauginos and Higgsinos. In summary, from this simple-minded scan we observe that for low to moderate values of $\tan\beta$, the branching ratios of the neutral Higgses H and A to a pair of charginos can be as large as 50%, while decay to a pair of neutralinos can be around 20%. Now, before we proceed to the next section, we would like to note a few important points. First, we find that these non-SM decay modes (i.e., Higgs decaying to electroweakinos) can be large enough, around 70–80%. However, so far we have not imposed the updated constraints on the various Higgs coupling measurements (usually expressed in terms of the signal strength variables) and the low-energy flavor data. Moreover, there exist strong bounds on the masses and couplings of the heavy Higgs bosons from the direct searches. In addition, both the ATLAS and CMS collaborations at the LHC have searched for the electroweakinos, and strong bounds exist from the LHC Run-I and Run-II data. In order to calculate the non-SM branching ratios of the heavy Higgses satisfying all the

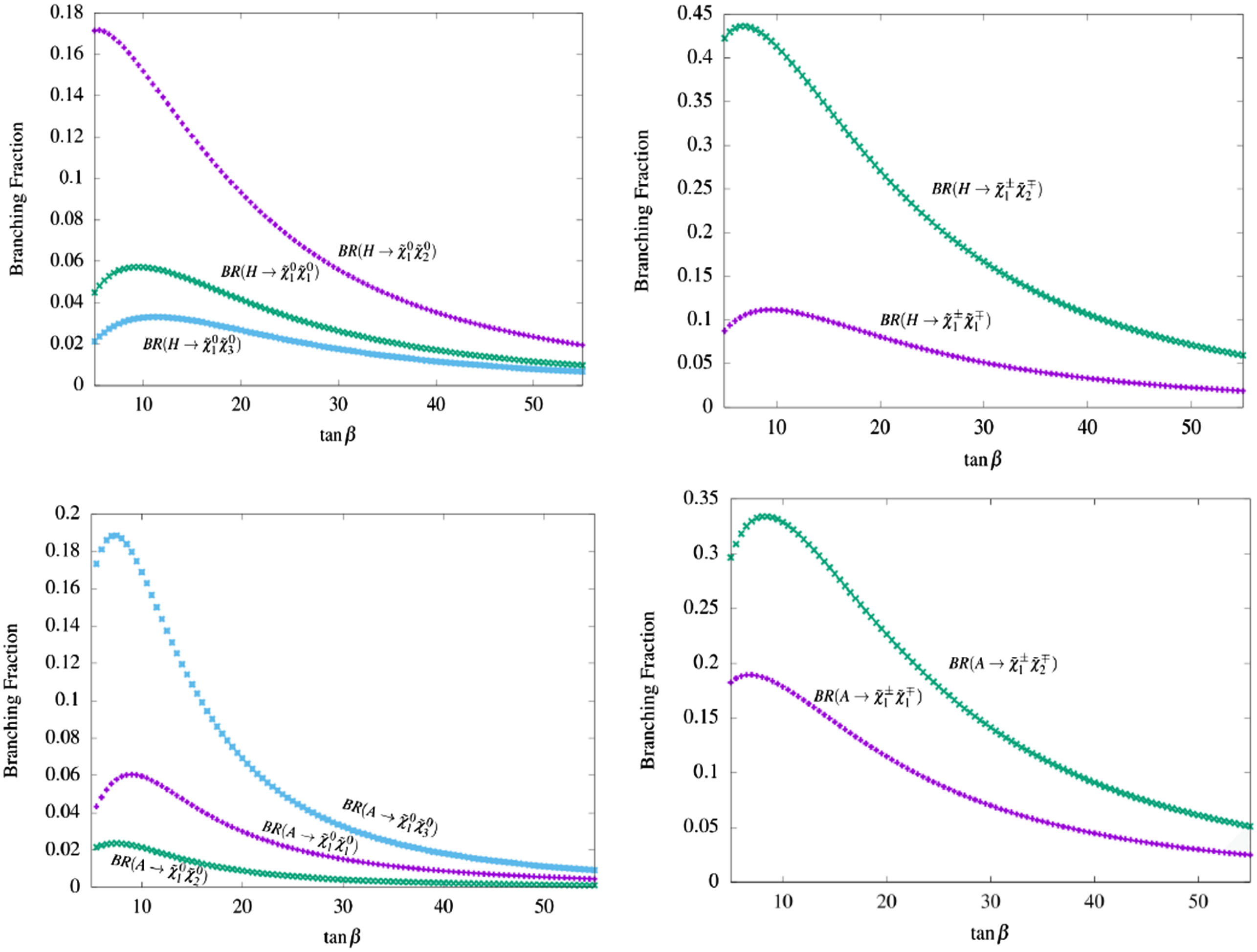

FIG. 2. The neutralino and chargino branching ratios of the heavy CP-even (upper panel) and CP-odd (lower panel) Higgs boson with respect to the variation of $\tan\beta$.

aforementioned collider constraints and low-energy flavor data, a dedicated scan involving the MSSM parameters is required to find the allowed parameter space, which is precisely the goal of the next section.

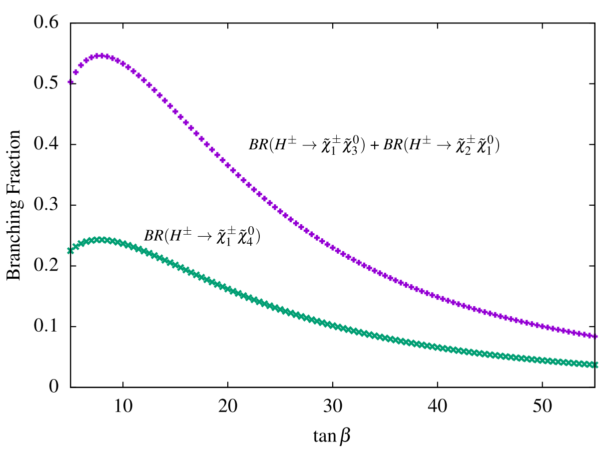

FIG. 3. The non-SM branching fractions of the charged Higgs boson with the variation of $\tan\beta$.

B. Experimental inputs and parameter-space scan

In this section we describe the parameter space scan along with the details of various experimental constraints considered in our analysis. After the completion of LHC Run-I, both the ATLAS and CMS collaborations at the LHC have published the combined results of 7 and 8 TeV Higgs data [3–5]. At the LHC, the main production mechanism of the Higgs boson (h) is the gluon-gluon fusion (ggF) process; however, other subdominant production mechanisms are vector-boson fusion (VBF), associated production with a W/Z boson (VH), and associated production with a pair of top quarks ($t\bar{t}h$). Both experimental collaborations have analyzed these processes for different decay modes of the Higgs boson, like $h \to \gamma\gamma$, $h \to WW^*$, $h \to ZZ^*$, $h \to b\bar{b}$, and $h \to \tau^+\tau^-$ [4,5]. These results are usually presented in terms of the signal strength variables (μ), defined as the ratio of the production cross section (σ) times the branching ratio (BR) for a specific production and decay mode of the candidate Higgs boson in a given new physics model normalized to the SM predictions, i.e.,

$$\mu_i^f = \frac{\sigma_i \times \mathrm{BR}^f}{(\sigma_i)_{\mathrm{SM}} \times (\mathrm{BR}^f)_{\mathrm{SM}}}, \tag{9}$$

where σ_i is the production cross section corresponding to a new physics model with $i = \mathrm{ggF}$, VBF, VH, and $t\bar{t}H$, with H being a generic Higgs boson and $f = \gamma\gamma, ZZ^*, WW^*, b\bar{b}, \tau^+\tau^-$ being the decay modes of the Higgs boson. The subscript "SM" represents the respective SM expectations. These signal strength variables should be measured very precisely as any small but statistically significant deviation from the SM will hint at possible signatures of beyond-the-SM physics. A combined analysis using 7 and 8 TeV data performed by the ATLAS and CMS collaborations has derived the constraints on the individual signal strength variables as well as in the $\mu^f_{\mathrm{ggF}+t\bar{t}h}, \mu^f_{\mathrm{VBF+VH}}$ plane through a ten-parameter fit corresponding to five decay modes of the Higgs boson [3]. The above-mentioned study has assumed that μ_V^f and μ_F^f do not change with the variation of the center-of-mass energy from 7 to 8 TeV. In our analysis, the MSSM parameter space obtained after the random scan has been constrained by using the 95% C.L. contours in the $\mu^f_{ggF+t\bar{t}h}, \mu^f_{\mathrm{VBF+VH}}$ plane, as presented in Fig. 28 of Ref. [3]. We study all five decay modes of the Higgs boson and those points which lie within the 95% C.L. contour are accepted for further analysis (see the Appendix for details).

In addition to the updated Higgs data, we also impose the current flavor physics constraints on $\mathrm{BR}(b \to s\gamma)$ and $\mathrm{BR}(B_s \to \mu^+\mu^-)$. In our analysis, we allow 2σ uncertainty on the measurement of these two most stringent rare b decays with respect to their current measured values $\mathrm{BR}(B_s \to X_s\gamma) = 3.43 \pm 0.22 \pm 0.21(\mathrm{theo})$ and $\mathrm{BR}(B_s \to \mu^+\mu^-) = 3.1 \pm 0.7 \pm 0.31(\mathrm{theo})$ [52], and assume

$$\begin{aligned} &2.82 \times 10^{-4} < \mathrm{BR}(\mathrm{B_s} \to \mathrm{X_s}\gamma) < 4.04 \times 10^{-4}, \\ &1.57 \times 10^{-9} < \mathrm{BR}(\mathrm{B_s} \to \mu^+\mu^-) < 4.63 \times 10^{-9}. \end{aligned} \tag{10}$$

We perform a random scan, restricting ourselves to the phenomenological MSSM. The parameters that are relevant to our study are mostly associated to the electroweakino sector and Higgs sector of the MSSM, namely the gaugino mass parameters $M_{1,2,3}$, the Higgsino mass parameter μ, the pseudoscalar mass parameter M_A, $\tan\beta$, the third-generation squark trilinear couplings A_t and A_b (the trilinear couplings of the sleptons and first two generations of squarks are set to zero), and the third-generation squark soft mass parameters M_{Q_3}, M_{U_3}, and M_{D_3}. Here we vary the parameters in the following ranges:

$$\begin{aligned} &1 < \tan\beta < 55, \qquad 150\ \mathrm{GeV} < M_A < 1\ \mathrm{TeV}, \\ &-10\ \mathrm{TeV} < A_\mathrm{t} < 10\ \mathrm{TeV}, \\ &1\ \mathrm{TeV} < M_{\mathrm{Q}_3}, M_{\mathrm{U}_3}, M_{\mathrm{D}_3} < 10\ \mathrm{TeV}, \\ &2\ \mathrm{TeV} < M_3 < 10\ \mathrm{TeV}, \end{aligned} \tag{11}$$

while we keep the soft parameters for the first two generations of squarks and all three generations of sleptons fixed at the values $M_{\mathrm{L}_{1,2,3}} = M_{\mathrm{E}_{1,2,3}} = M_{\mathrm{Q}_{1,2}} = M_{\mathrm{U}_{1,2}} = M_{\mathrm{D}_{1,2}} = 3$ TeV, where $M_{\mathrm{L_i}}$ and $M_{\mathrm{E_i}}$ ($i = 1, 2, 3$) are the left- and right-handed slepton soft SUSY-breaking mass parameters, and $M_{\mathrm{Q_i}}$, $M_{\mathrm{U_i}}$, $M_{\mathrm{D_i}}$ ($i = 1, 2$) are the first two generations of squark soft SUSY-breaking mass parameters. The parameters M_1, M_2, μ are varied according to some specific assumptions, as discussed below.

We scan over a wide range of the above-mentioned parameters in order to obtain the lightest MSSM Higgs boson mass in the range of 125 ± 3 GeV assuming a 3 GeV uncertainty in the Higgs mass calculation [53]. To scan the MSSM parameter space we use SUSPECT and branching ratios of the Higgs boson are evaluated using HDECAY. For the estimation of various branching ratios of the SUSY particles (specially electroweakinos), we use SUSYHIT (version 1.5) [54]. The flavor physics observables are calculated using MICROMEGAS (version 4.1.8) [55]. Depending on the region of our interest, we consider ten different types of models, each differing by the values of the parameters associated to the electroweakino sector, namely, M_1, M_2, and μ.

Let us reiterate that the point of this paper is to study the SUSY cascade decays of the MSSM heavy Higgses to the electroweakinos. So the parameters of interest are the M_1 (bino), M_2 (wino), and μ (Higgsino) mass parameters which are associated to the chargino and neutralino sector of the MSSM. Here we consider various possible combinations of these bino (B), wino (W), and Higgsino (H) mass parameters and construct several representative models. From Model-B to Model-BWH we vary the parameters M_1, M_2, and μ by choosing all possible combinations among them (see Tables I–II). The name of each model signifies the nature of the lightest electroweakino particle, except Model-BWH. For example, "Model-X" reflects the fact that the mass parameter "X" is the lightest among all the gaugino and Higgsino mass parameters. Similarly, the model "Model-XY" denotes that both X and Y are varied independently within the specified range, however, with the condition that X is always smaller than Y, i.e., $X < Y$. A most general framework where no specific assumptions have been imposed on those parameters is labeled as Model-BWH in Table II. In all of these representative models, except for Model-BWH, the lightest gaugino/Higgsino mass parameter is allowed to vary up to $M_A/2$, as for heavier electroweakinos the decay of the MSSM heavy Higgses to these modes will be kinematically forbidden. The lower values of some of these scanning parameters are determined from existing LEP bounds [56]. Here, the pseudoscalar mass M_A has been varied from 150 GeV to 1 TeV in order to obtain a wide spectrum of the MSSM heavy Higgs boson masses.

TABLE I. Representative models for different possible hierarchies among the gaugino and Higgsino mass parameters. In all of these cases the pseudoscalar mass parameter has been varied between 150 GeV $< M_A <$ 1000 GeV. "Model-X" denotes the case where the mass parameter "X" is the lightest among all the gaugino and Higgsino mass parameters, while "Model-XY" represents the scenario when both X and Y are varied independently within the specified range, however, with the condition $X < Y$.

Model Name	Parameter varied	Fixed parameters	Mass hierarchy	Range(s) of variation
Model-B	M_1	$M_2 = \mu = 2$ TeV	$M_2, \mu \gg M_1$	1 GeV $< M_1 < M_A/2$
Model-W	M_2	$M_1 = \mu = 2$ TeV	$M_1, \mu \gg M_2$	100 GeV $< M_2 < M_A/2$
Model-H	μ	$M_1 = M_2 = 2$ TeV	$M_1, M_2 \gg \mu$	100 GeV $< \mu < M_A/2$
Model-BW	M_1, M_2	$\mu = 2$ TeV	$\mu \gg M_2 > M_1$	100 GeV $< M_1 < M_A/2$ $M_1 < M_2 < M_A$
Model-WB	M_1, M_2	$\mu = 2$ TeV	$\mu \gg M_1 > M_2$	100 GeV $< M_2 < M_A/2$ $M_2 < M_1 < M_A$

TABLE II. Representative models for different possible hierarchies among the gaugino and Higgsino mass parameters. In all of these cases the pseudoscalar mass parameter has been varied between 150 GeV $< M_A <$ 1000 GeV. "Model-XY" represents the fact that both X and Y have been varied independently within the specified ranges, however, with the condition $X < Y$. The last representative model Model-BWH, however, represents a most general scenario when no specific mass hierarchy among the gaugino and Higgsino mass parameters has been imposed; it just denotes the fact that here all the parameters are varied independently.

Model Name	Parameter varied	Fixed parameters	Mass hierarchy	Range(s) of variation
Model-BH	M_1, μ	$M_2 = 2$ TeV	$M_2 \gg \mu > M_1$	1 GeV $< M_1 < M_A/2$ $M_1 < \mu < M_A$
Model-HB	M_1, μ	$M_2 = 2$ TeV	$M_2 \gg M_1 > \mu$	100 GeV $< \mu < M_A/2$ $\mu < M_1 < M_A$
Model-WH	M_2, μ	$M_1 = 2$ TeV	$M_1 \gg \mu > M_2$	100 GeV $< M_2 < M_A/2$ $M_2 < \mu < M_A$
Model-HW	M_2, μ	$M_1 = 2$ TeV	$M_1 \gg M_2 > \mu$	100 GeV $< \mu < M_A/2$ $\mu < M_2 < M_A/2$
Model-BWH	M_1, M_2, μ	… …	… …	100 GeV $< M_2, \mu <$ 1000 GeV 100 GeV $< M_1 <$ 1000 GeV

C. SUSY decay of heavy Higgses and the allowed parameter space

In this section we discuss the results obtained after the parameter space scan for the representative models introduced in the last section and estimate various branching ratios of the heavy Higgses H, A, $H^{\pm}$ to electroweakinos. Here we would like to remind our readers that these branching fractions (or, say, couplings of heavy Higgses to electroweak gaugino/Higgsino states) crucially depend on the mixing between electroweak gaugino and Higgsino states and, in fact, an almost pure Higgsino or gaugino state will have highly suppressed branching ratios with respect to the mixed states. This very feature has been observed for all of these representative models (Model-B–Model-BWH). For example, for Model-B, Model-W, Model-BW, and Model-WB the neutralinos and charginos are almost purely gaugino-like, while for Model-H they are purely Higgsino-like, and thus they offer a very negligible amount of mixing between the gaugino and Higgsino states. Due to this minuscule mixing, we obtain highly suppressed (∼2%) branching fractions for all the heavy Higgses (H, A, $H^{\pm}$) decaying to neutralino and chargino states. In Table III, we summarize the maximum allowed branching ratios for the heavy Higgses, summing individual decay modes of a given Higgs boson to different neutralino and chargino states.

For Model-B to Model-WB (as defined in Table I) by construction we have a negligible amount of gaugino-Higgsino mixing and thus the observation of the highly suppressed branching ratios of the heavy Higgses to various neutralino/chargino states is well understood. Below, however, we allow significant gaugino-Higgsino mixing by modifying the parameters and construct five more representative models—Model-BH to Model-BWH—and estimate the individual non-SM branching ratios. In Fig. 4, we plot the maximum possible value of a non-SM branching ratio, out of all possible modes, obtained for a particular value of $\tan\beta$ in the context of all five representative scenarios Model-BH to Model-BWH (as defined in Table II). Due to large mixing between Higgsinos and gauginos, we find that various "ino" branching ratios can be as large as 40–80%. However, it is to be noted that, when

TABLE III. The branching ratios of the heavy Higgses (H, A, and $H^{\pm}$) to various charginos and neutralinos. The numbers represent the sum of decay modes of the given Higgs boson to all possible neutralino-neutralino, neutralino-chargino, and chargino-chargino states for Model-B to Model-WB with the indices i, $j = 1, 2, 3, 4$ and k, $\ell = 1, 2$.

	Model-B	Model-W	Model-H	Model-BW	Model-WB
$H \to \tilde{\chi}_i^0 \tilde{\chi}_j^0$	≤0.07	≤0.7	≤0.65	≤1.2	≤1.2
$H \to \tilde{\chi}_k{}^{\pm} \tilde{\chi}_\ell{}^{\mp}$	∼0	≤1.4	≤1.3	≤1.3	≤1.4
$A \to \tilde{\chi}_i^0 \tilde{\chi}_j^0$	≤0.07	≤0.8	≤0.7	≤1.4	≤1.4
$A \to \tilde{\chi}_k{}^{\pm} \tilde{\chi}_\ell{}^{\mp}$	∼0	≤1.6	≤1.5	≤1.6	≤1.6
$H^{\pm} \to \tilde{\chi}_i^0 \tilde{\chi}_k{}^{\pm}$	∼0	∼0	≤0.25	≤1	≤1

both decays are kinematically allowed, the decay of the neutral (both CP-even and -odd) Higgses to a pair of charginos dominates over the decays to a pair of neutralinos. Moreover, when the wino-Higgsino mixing is large compared to bino-Higgsino mixing by setting M_2 and μ sufficiently light while M_1 is decoupled, the non-SM decay modes can be significantly large. The enhancement is mostly driven by the large branching ratio to the chargino pairs.

We are now in a position to discuss salient features of various representative models in detail. We start with Model-BH and subsequently discuss other models, and also compare the results. In Model-BH, we assume $M_2 \gg \mu > M_1$ with M_2 fixed at 2 TeV, and thus our choice pushes the masses of $\tilde{\chi}_4^0$ and $\tilde{\chi}_2{}^{\pm}$ to 2 TeV. One can now expect to see several possible final-state signatures involving lighter neutralinos and charginos, for example, H/A decaying to $\tilde{\chi}_1^0\tilde{\chi}_2^0$, $\tilde{\chi}_1^0\tilde{\chi}_3^0$, $\tilde{\chi}_2^0\tilde{\chi}_3^0$, $\tilde{\chi}_1^0\tilde{\chi}_1^0$, $\tilde{\chi}_2^0\tilde{\chi}_2^0$, $\tilde{\chi}_3^0\tilde{\chi}_3^0$, etc. In Fig. 5, we present branching ratios to these various final-state topologies with the variation of $\tan\beta$. In the case when Higgs H/A decays to a pair of neutralinos $H/A \to \tilde{\chi}_i^0\tilde{\chi}_j^0$ with $i \neq j$, the branching fractions can be as large as 20% each, while

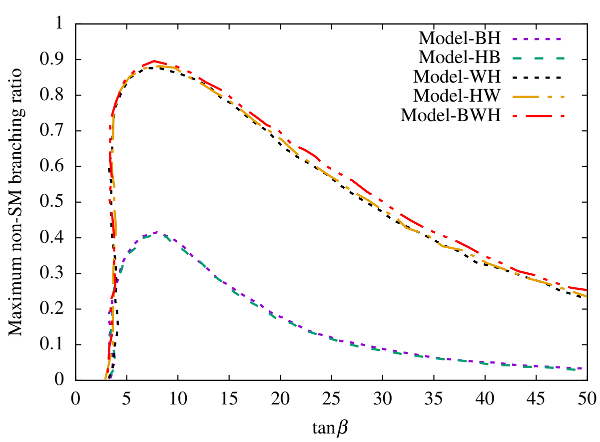

FIG. 4. The non-SM branching ratios for Model-BH to Model-BWH (as defined in Table II) for different values of $\tan\beta$. Here we calculate the maximum possible value of a non-SM "ino" branching fraction among all possible "ino" decay modes of the heavy CP-even Higgs boson (H).

for $i = j$ it is somewhat smaller (for $i = j = 1$, it is around 10–15%). Decay to a pair of charginos is also possible and, in fact, it can be dominant compared to the neutralino modes depending upon the choices of the parameters. In Fig. 6 we show various branching fractions of the H (left panel) and A (right panel) bosons to a pair of charginos and, as can be clearly seen, these branching ratios are highly suppressed (less than 1%); this is due to the negligibly small mixing between the Higgsino and wino components, and thereby the lightest chargino is dominantly Higgsino-like while the heavier one is gaugino-like. The final states of the charged Higgs decay include a chargino-neutralino pair, and from Fig. 7 we see that these modes can also be sufficiently large for lower values of $\tan\beta$. In fact these branching fractions can go up to ∼35% ($\tilde{\chi}_1{}^{\pm}\tilde{\chi}_1^0$) and ∼20% ($\tilde{\chi}_1{}^{\pm}\tilde{\chi}_3^0$), respectively, when the lightest chargino state is Higgsino-like and the lightest neutralino state is gaugino-like. We note in passing that the large branching ratios to these "ino" modes will lead to interesting collider signatures through cascade decays that can be tested at the ongoing and future runs of the LHC.

Having discussed Model-BH in detail, let us now interchange the hierarchy of M_1 and μ while keeping M_2 decoupled, i.e., $M_2 \gg M_1 > \mu$ (Model-HB), and see how the results change. We find that the distributions and various properties are almost the same as those of Model-BH, except for the fact that the $\tilde{\chi}_1^0$ and $\tilde{\chi}_2^0$ are now Higgsino dominated and $\tilde{\chi}_3^0$ is now bino dominated (for close values of M_1 and μ these states are an admixture of bino-Higgsino). Hence, compared to Model-BH, here the $\mathrm{BR}(H \to \tilde{\chi}_2^0\tilde{\chi}_3^0)$ and $\mathrm{BR}(A \to \tilde{\chi}_1^0\tilde{\chi}_3^0)$ dominate and $H/A \to \tilde{\chi}_1^0\tilde{\chi}_2^0$ has relatively small branching ratios. The charged Higgs branchings to electroweakinos are also in the same ballpark of Model-BH. In the low-$\tan\beta$ region, the maximum BRs of $H^{\pm}$ are about 35% for $\tilde{\chi}_1{}^{\pm}\tilde{\chi}_3^0$ and 20% for $\tilde{\chi}_1{}^{\pm}\tilde{\chi}_1^0$.

One can also assume a possible hierarchy between the model parameters as $M_1 \gg \mu > M_2$ (Model-WH) or $M_1 \gg M_2 > \mu$ (Model-HW). The difference between these two scenarios is that in the first case the LSP is wino dominated (Model-WH), while in the second case the LSP is Higgsino dominated (Model-HW). We find that, depending on the

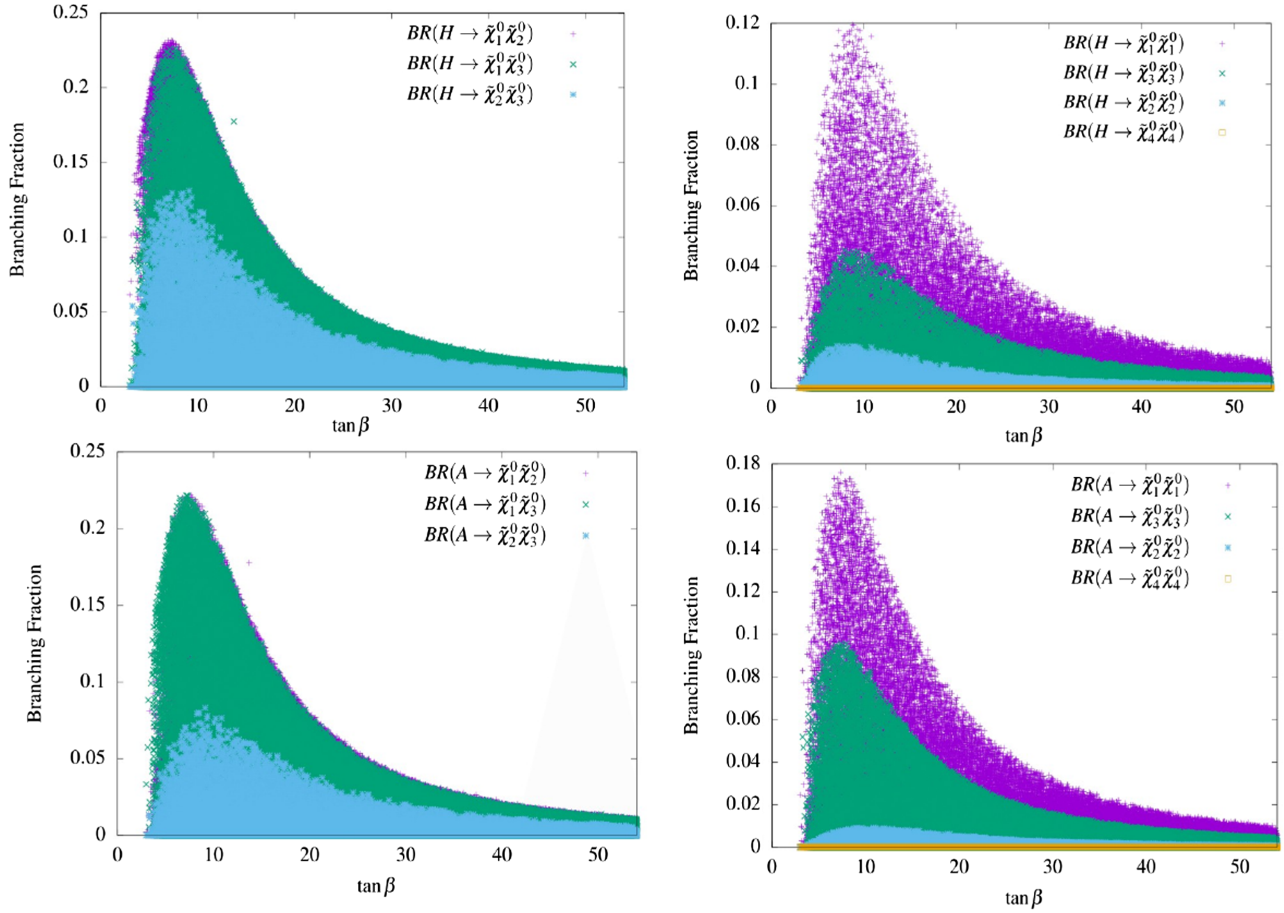

FIG. 5. Branching fractions of the heavy Higgs bosons H and A to various neutralinos in the context of Model-BH.

wino-Higgsino mixing and the values of $\tan\beta$, heavy Higgs decay to a pair of neutralinos and/or charginos can reach up to 10–25%. However, due to the presence of light charginos in the particle spectrum and large Higgsino-wino mixing, heavy Higgs decay to a pair of charginos can be as large as 50% for both Model-WH and Model-HW. Moreover, we also find that the charged Higgs decay to a chargino-neutralino pair is also possible (with BR $\sim 25\%$) in the entire region of the parameter space for low to moderate values of $\tan\beta$.

Given the three free input parameters M_1, M_2 and μ, one is not always forced to assume a specific hierarchy between them; instead, one can always take a simple-minded approach and allow all of them to vary independently. This is precisely our last representative model, namely Model-BWH, where we scan for all possible values of M_1,

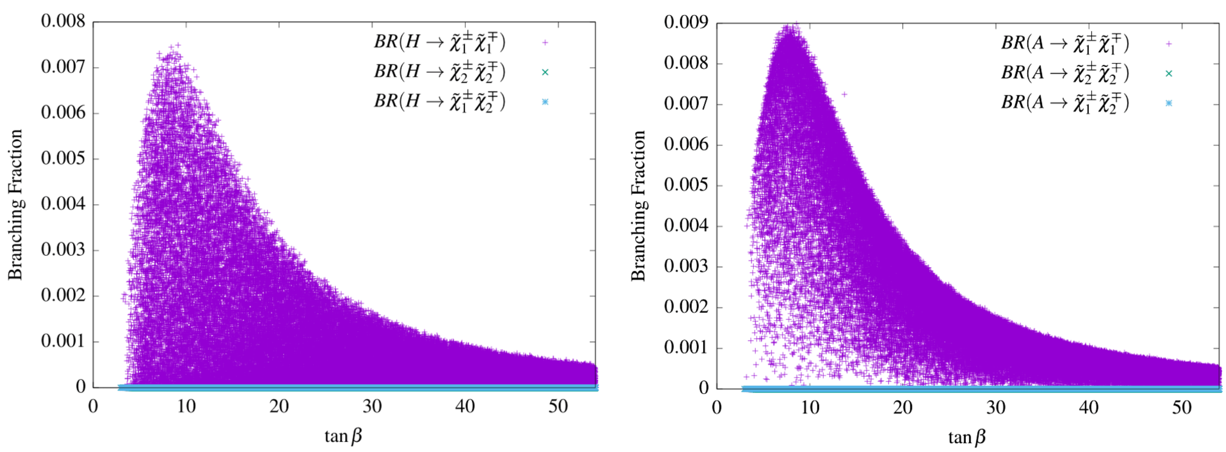

FIG. 6. Branching fractions of the heavy Higgs bosons H and A to the charginos in the context of Model-BH.

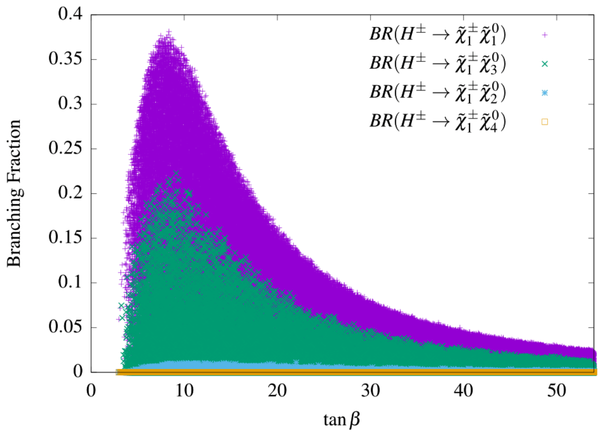

FIG. 7. The decay of the charged Higgs boson $H^\pm$ to chargino-neutralino final states, where we consider Model-BH.

M_2, and μ without imposing any hierarchy among them. The added advantage of this kind of choice is that many decay modes that were not kinematically allowed earlier will now open up, and thus make it phenomenologically richer. For example, the presence of small M_1, M_2, and μ implies that the decay modes containing $\tilde{\chi}_4^0$ are now accessible in some parts of the parameter space. Again, however, the magnitude of the individual decay modes will crucially depend upon the values of M_1, M_2, and μ. In Fig. 8, we display all the possible decay modes of the heavy neutral and charged Higgs bosons to final states with charginos and neutralinos for Model-BWH. From the distributions one can observe an appreciable amount of enhancement in heavy Higgs branching fractions for some of the decay modes which were absent in our earlier constructions (say, Model-B to Model-WB). Interestingly, in all of these cases long cascade decays originating from heavy Higgs decay may result in testable collider

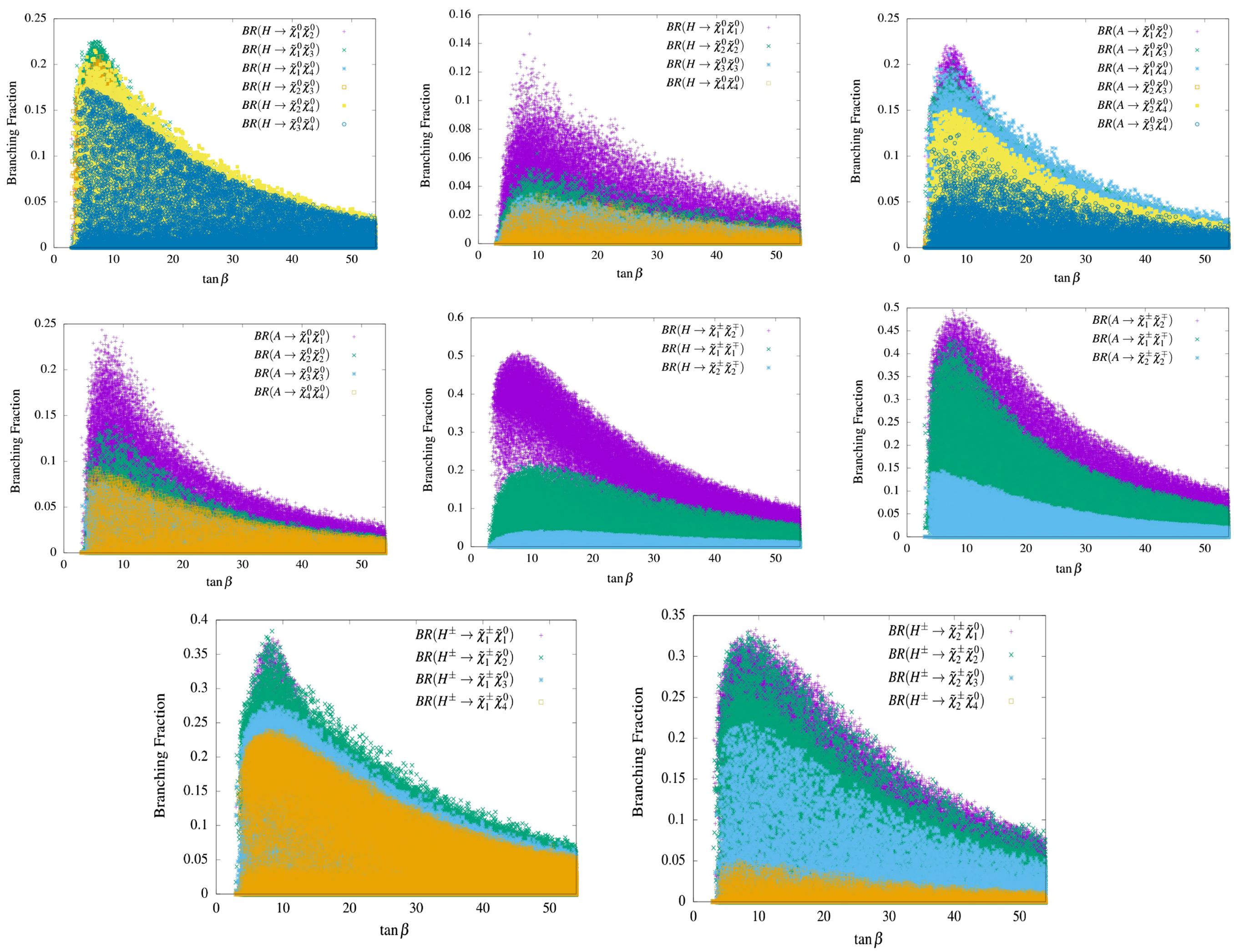

FIG. 8. Branching ratios for heavy Higgses (neutral and charged) decaying to various chargino and neutralino final states in the context of Model-BWH.

signatures, starting from relatively simpler signatures like mono-Z/mono-W/mono-h/dibosons plus $\not{E}_T$ signatures, to relatively complex final-state topologies consisting of multiple leptons, jets, and $\not{E}_T$. Before moving on to the next section, we would like to note that we also obtain some parameter space points where the charginos are heavier than the light top squark (≈ 3 in 10^4 points). Under these circumstances, the chargino can dominantly decay to the light top squark and a bottom quark; in fact, in some cases one can observe a $\mathrm{Br}(\tilde{\chi}_1^{\pm} \to \tilde{t}_1 b)$ as large as 90%, depending upon the relative values of the input parameters.

For the rest of our analysis, we consider those benchmark models where these heavy Higgses have an appreciable amount of branching fractions to charginos and neutralinos, and thus we restrict ourselves within Model-BH to Model-BWH. However, before we advance towards the detailed collider analysis, we would like to remind our readers that there exists an avalanche of studies where both the ATLAS and CMS collaborations at the LHC have searched for heavy scalar resonances through different final-state signatures. Moreover, direct searches for the electroweakinos have also been performed at the LHC. However, it is difficult to incorporate all these LHC constraints into our parameter-space scan. Thus, in order to enliven our analysis, we choose a few representative benchmark points which are allowed by the current LHC data and then perform the detailed collider analysis.

D. Current LHC bounds for the heavy Higgs sector and electroweakinos

In this section we summarize the relevant LHC constraints originating mainly from the LHC Run-I data and also a few from the early 13 TeV Run-II data. We start by discussing the current bounds on the masses and branching ratios of the heavy neutral and charged Higgs bosons obtained by the ATLAS and CMS collaborations for various possible final states, and then proceed to outline the present constraints on the electroweakinos from the Run-I data.

1. Search for H with $\gamma\gamma$ final states

The diphoton invariant mass distribution can be a useful probe to search for the additional Higgses. Both the ATLAS and CMS collaborations have looked for scalar particles decaying via narrow resonances into a two-photon final state using the Run-I data [11,12]. The ATLAS (CMS) Collaboration has performed the study using 20.3(19.7) fb^{-1} data in the mass range 65–600 (150–850) GeV and no significant excess over the SM background has been observed. The results have been presented as 95% C.L. upper limits on the production cross section times branching ratio into a pair of photons, i.e., the limit on the quantity $\sigma \times \mathrm{Br}(H \to \gamma\gamma)$. For example, the upper limit[2] on $\sigma \times \mathrm{Br}(H \to \gamma\gamma)$ for a heavy Higgs with mass $M_H = 600$ GeV as obtained by ATLAS is around 1 fb [11].

Recently, both the ATLAS and CMS collaborations have reported an excess in the diphoton invariant mass distribution around 750 GeV with the early 13 TeV data [57,58]. The local significance of the excess observed by CMS is approximately 3.4σ combining 8 TeV 19.7 fb^{-1} data and 13 TeV 3.2 fb^{-1} data [58]. ATLAS has also observed the excess with local significance 3.9σ for about a 50 GeV decay width of the heavy resonance [57]. In our work, we use the 95% C.L. upper limits on the production cross section times branching ratio for different choices of heavy resonance masses as derived by both experimental collaborations.

2. Search for H with WW final states

Searches for a high-mass Higgs boson in the $H \to WW \to \ell\nu\ell\nu$ and $H \to WW \to \ell\nu qq$ decay channels have been performed by the ATLAS and CMS collaborations using the LHC Run-I data [13,14]. In the absence of evidence of a signal, the upper limits on $\sigma \times \mathrm{Br}(\mathrm{H} \to \mathrm{WW})$ as a function of m_H are reported for different possible choices of the width (Γ_H) of the Higgs boson. The ATLAS study has been performed using 20.3 fb^{-1} data in the mass range 200–1500 GeV [13] with 8 TeV data. CMS has also performed the same analysis using the complete data set ($5.1 + 19.7$ fb^{-1}) collected at $\sqrt{s} = 7$ and 8 TeV data in the mass range $145 < m_H < 1000$ GeV [14]. Here we would like to note that as we proceed near the alignment limit [59] [i.e., $(\beta - \alpha) \sim \frac{\pi}{2}$ with α being the Higgs mixing angle], $\mathrm{BR}(H \to WW)$ becomes highly suppressed and then the bound on $\sigma \times \mathrm{Br}(H \to WW)$ becomes less significant for most of the MSSM parameter space (see Fig. 7b of Ref. [60] for more details). The ATLAS Collaboration has also looked for a heavy neutral scalar particle decaying into a pair of W bosons, and placed upper limits on $\sigma \times \mathrm{Br}(H \to WW)$ as a function of m_H in the entire mass range of 600 GeV to 3 TeV using the LHC Run-II data with $\mathcal{L} = 3.2$ fb^{-1} luminosity [61].

3. Search for H with ZZ final states

Searches for additional Higgses in the ZZ channel have also been reported by the ATLAS and CMS collaborations [14,15,62]. The analysis by ATLAS with 20.3 fb^{-1} of 8 TeV data focused on the four final-state topologies: $H \to ZZ \to \ell^+\ell^-\ell^+\ell^-$, $\ell^+\ell^-\nu\bar{\nu}$, $\ell^+\ell^- q\bar{q}$, $\nu\bar{\nu}q\bar{q}$ in the mass range 140–1000 GeV [15]. It is needless to mention that better tagging efficiency leads to 4ℓ being the most sensitive channel. In the absence of any significant excess

[2]Note that ATLAS has obtained an upper limit on fiducial cross section (σ_{fid}) times branching ratio, where σ_{fid} includes an efficiency correction factor [11].

the 95% C.L. upper limits on $\sigma \times \mathrm{Br}(H \to ZZ)$ for the two production modes of the Higgs boson (ggF and VBF) are obtained by combining all four search channels with the narrow-width approximation.

The same topology has been searched by the CMS Collaboration using $(5.1 + 19.7\ \mathrm{fb}^{-1})$ data collected during the $\sqrt{s} = 7$ and 8 TeV LHC run focusing on the mass range $145 < m_H < 1000$ GeV [14]. The 95% C.L. exclusion limits for different final states were also presented. Recently the ATLAS Collaboration has performed a search for a heavy Higgs with a $H \to ZZ \to \ell^+\ell^- q\bar{q}$ final state using 3.2 fb^{-1} of Run-II data. Nonobservation of a signal leads to 95% C.L. limits on $\sigma \times$ BR in the entire mass range 300–1000 GeV [62]. It is to be noted that, similarly to the $H \to WW$ mode, $\mathrm{Br}(H \to ZZ)$ also gets highly suppressed as one approaches the alignment limit as both couplings are proportional to $\cos(\beta - \alpha)$.

4. Search for H with hh final states

The heavy Higgs decay to a pair of SM Higgses $H \to hh$ is significant only for low $\tan\beta$ ($\lesssim$10) and low to moderate values of $M_A \leq 400$ GeV. At higher values of M_A and low values of $\tan\beta$, the $H \to t\bar{t}$ channel dominates, and thereby all other decay modes get highly suppressed. Depending on the choice of the model parameters, the production cross section of a single *CP*-even Higgs can be up to 2 orders of magnitude larger compared to the direct *hh* production (see Table 1 of Ref. [63]) and it can also have nontrivial effects on the self-coupling measurement of the 125 GeV Higgs [63]. The search for resonant production of a pair of SM Higgses has been done by both the ATLAS and CMS collaborations with 8 TeV data assuming various final-state topologies, like $b\bar{b}b\bar{b}$ [16,17], $b\bar{b}\gamma\gamma$ [18,19], $b\bar{b}\tau\tau$ [20], and $WW\gamma\gamma$ [20]. In fact, in Ref. [20] ATLAS has combined the results for the four above-mentioned channels and presented the observed and expected 95% C.L. upper limits on $\sigma \times \mathrm{Br}(H \to hh)$ at $\sqrt{s} = 8$ TeV (see Fig. 6 of Ref. [20]). Among the four decay modes, $hh \to b\bar{b}b\bar{b}$ dominates because of the large branching ratio of $h \to b\bar{b}$. However, the reconstruction of the $b\bar{b}b\bar{b}$ final state is rather complex because of the large QCD multijet background. Thus, less dominant modes like the $b\bar{b}\gamma\gamma$ channel become the most sensitive in the low and relatively heavy (500 GeV) mass region, as it has comparatively less background and better mass resolution. The CMS Collaboration has investigated both channels, $H \to hh \to b\bar{b}b\bar{b}$ and $H \to hh \to b\bar{b}\gamma\gamma$, for the mass range 260 GeV $\leq M_H \leq 1.1$ TeV using LHC-8 data [17,19]. The ATLAS analyses focused on two different mass regions: for $b\bar{b}b\bar{b}$ they restricted themselves to 500–1500 GeV, while for $b\bar{b}\gamma\gamma$ they targeted the 260–500 GeV mass regime [16,18]. In the absence of signal events, both ATLAS and CMS have put 95% C.L. upper limits on the production cross section times branching fraction of the heavy resonance for different mass ranges.

5. Search for H/A with $\tau^+\tau^-$ final states

The search analysis with $H/A \to \tau^+\tau^-$ is one of the most important and most promising channels to constrain the MSSM parameter space. The LHC Run-I data has already severely constrained the MSSM parameter space with large to moderate values of $\tan\beta$, say $\gtrsim$15, using the $H \to \tau^+\tau^-$ channel. The reason why regions with large values of $\tan\beta$ are excluded is primarily because of the heavy Higgses H, A coupling with the SM fermions. For example, the coupling of H, A with down (up) type fermions b, τ (t) increases (decreases) with $\tan\beta$ and thus the dominant production modes of H/A (mainly ggF and associated production with $b\bar{b}$) are primarily controlled by $\tan\beta$. Both the ATLAS and CMS collaborations have looked for signatures of H/A produced via ggF and $b\bar{b}\Phi$ ($\Phi = H$, A) processes with the Higgs decaying to $\tau^+\tau^-$ [23,24] with LHC-8 data. Nonobservation of significant excess over the SM backgrounds results in model-independent 95% C.L. upper limits on $\sigma \times \mathrm{Br}(\Phi \to \tau^+\tau^-)$ for different values of M_Φ with $\Phi = H/A$ at 95% C.L.

Recent results from the ATLAS (CMS) experiment have been reported with final states containing a tau pair using the data recorded during 2015 at a center-of-mass energy of 13 TeV with $\mathcal{L} = 3.2(2.3)\ \mathrm{fb}^{-1}$ [64,65]. Both collaborations have seen a very good agreement between the data and the SM backgrounds. As a result of this agreement 95% C.L. upper limits on the production cross section times branching fraction have been placed. Now, if one translates these experimental upper bounds in terms of the model parameters—say, for the MSSM in the $M_A - \tan\beta$ plane—and compare the Run-II data with the existing Run-I data, one can clearly observe an appreciable improvement in the Run-II data for regions with $M_A > 700$ GeV, while in the rest of the parameter space Run-I and Run-II are already comparable.

6. Search for A with Zh final states

The decay of a pseudoscalar boson A to Zh is kinematically allowed and becomes appreciable with M_A below the $t\bar{t}$ threshold (i.e., <350 GeV) and very low values of $\tan\beta$ (<10). Both the ATLAS and CMS collaborations have investigated this final-state topology with h decaying to $b\bar{b}$ (ATLAS has also analyzed the $h \to \tau\tau$ mode [21]) and a Z boson into a pair of oppositely charged leptons (electrons or muons) with 8 TeV data [21,22]. A similar sort of analysis has also been looked at recently by the ATLAS Collaboration with 3.2 fb^{-1} of Run-II data [66]. From all of these analyses, nonobservation of any signal of an A boson leads to an upper limit on the production cross section times branching ratio for a wide range of pseudoscalar masses.

7. Search for $H^{\pm}$ with $\tau\nu$ and $t\bar{b}$ final states

The observation of a charged Higgs boson signal is one of the smoking gun signatures of physics beyond the SM. From the direct searches at the LEP collider, charged Higgs masses have to be greater than around 80 GeV [56]. At the LHC, the search strategies of charged Higgses crucially depend on its mass; in other words, when the charged Higgs is light ($M_{H^{\pm}} < M_{\rm top}$) it is primarily produced from the $t\bar{t}$ process and decays into $\tau\nu_{\tau}$ final states. However, for heavy $H^{\pm}$ ($M_{H^{\pm}} > M_{\rm top}$), they are mainly produced in associated production with top and bottom quarks, i.e., $pp \to tbH^{\pm}$.

Both the ATLAS and CMS collaborations have searched for light $H^{\pm}$, produced through $t\bar{t}$ processes and decaying to $c\bar{s}$ and $\tau\nu_{\tau}$ final states with LHC-8 data [25,26,28]. Search for heavy charged Higgs via $H^{\pm} \to t\bar{b}$ channel with multi b-jets in the final states has also been studied [26,29]. Again, nonobservation of any excess over the SM predictions leads to 95% C.L. exclusion limits on the production cross section times branching ratios for different values of $M_{H^{\pm}}$. From the exclusion limits, we find that regions with very high $\tan\beta$ (>20–25) are only severely constrained for relatively large values of the charged Higgs mass. Recently, the ATLAS Collaboration presented the early Run-II results for $H^{\pm}$ decaying into $\tau\nu$ final states with the $\mathcal{L} = 3.2\ \text{fb}^{-1}$ data set corresponding to $\sqrt{s} = 13$ TeV [67]. However, similar to the Run-I data, they again placed 95% C.L. upper limits on $\sigma \times \text{Br}$ which are very much similar to the existing 8 TeV bounds.

8. Current LHC bounds for electroweakinos

The relatively smaller production cross section of the electroweak sparticles—namely, charginos, neutralinos, and sleptons—results in comparatively weaker bounds on their masses and couplings compared to the colored SUSY particles. However, with the 8 TeV data, the ATLAS and CMS collaborations have already placed strong constraints on the masses/couplings through direct searches of the electroweakinos [68–74]. The mass bounds obtained by ATLAS and CMS are mostly based on simplified SUSY scenarios. However, we know that these bounds crucially depend on the hierarchy between the slepton and the gaugino masses, the composition of the electroweakinos, and most importantly on their branching ratios.[3] The majority of these searches assume a bino-like LSP, while the second lightest neutralino ($\tilde{\chi}_2^0$) and the lighter chargino ($\tilde{\chi}_1^{\pm}$) are purely wino-like [68–74]. In fact, the most significant bound is obtained from the $\tilde{\chi}_1^{\pm}\tilde{\chi}_2^0$ pair-production process with a trilepton plus missing energy ($\not{E}_{\rm T}$) signature [68,74].

[3]In most of the analysis, the LHC collaborations assumed a 100% branching ratio into one particular decay mode.

In our work we assume sleptons to be sufficiently heavy (masses around 3 TeV), and thus the electroweakinos mainly decay via W, Z, h bosons. With the decoupled scenario the limits become much weaker compared to the scenarios with intermediate lighter sleptons.[4] For wino-dominated $\tilde{\chi}_1^{\pm}$ and $\tilde{\chi}_2^0$ decaying 100% to $\tilde{\chi}_1^{\pm} \to \tilde{\chi}_1^0 W^{\pm}$ and $\tilde{\chi}_2^0 \to \tilde{\chi}_1^0 Z$ and with decoupled sleptons, the mass limits on charginos obtained by the ATLAS and CMS collaborations are 350 GeV for a massless LSP and 305 GeV for $m_{\tilde{\chi}_1^0} = 125$ GeV. However, note that the limits entirely vanish for $m_{\tilde{\chi}_1^0} > 125$ GeV. The exclusion limits are weakest when $\tilde{\chi}_2^0$ decays via the *spoiler* mode ($h\tilde{\chi}_1^0$) [71,72,74]. Moreover, degenerate chargino-neutralino masses up to 148 GeV are excluded for LSP masses up to 20 GeV when the decay modes of neutralinos involve a Higgs boson through a trilepton + $\not{E}_{\rm T}$ signature. Furthermore, the ATLAS Collaboration has also presented the electroweakino searches with $1\ell + 2b$ and $1\ell + 2\gamma$ ($\ell = e, \mu$) final states [71] for simplified models with the assumption $\text{BR}(\tilde{\chi}_2^0 \to \tilde{\chi}_1^0 h) = 100\%$. The limit obtained from the $1\ell + 2\gamma$ ($\ell = e, \mu$) channel is a little bit stronger than the trilepton bounds. However, it is to be remembered that the sharing of the branching ratios between $\tilde{\chi}_1^0 h$ and $\tilde{\chi}_1^0 Z$ can modify the exclusion limits considerably; for details we refer to the recent study [76].

In this work, we consider the present LHC constraints[5] on the electroweakinos via the $3\ell + \not{E}_{\rm T}$, $1\ell + 2b + \not{E}_{\rm T}$, and $1\ell + 2\gamma + \not{E}_{\rm T}$ ($\ell = e, \mu$) channels obtained by the ATLAS Collaboration with the LHC-8 data. To study[6] the impact of these constraints on our parameter space, we first calculate the signal and background efficiencies for some representative benchmark points (see next section), and then using the next-to-leading-order (NLO) production cross sections as obtained from PROSPINO [77] we estimate the effective cross sections and then make sure that our numbers lie below the 95% C.L. upper limits already presented by the ATLAS Collaboration in the three above-mentioned channels.

III. SEARCH STRATEGIES AND FUTURE LIMITS

From the previous section, we find that the branching fraction of the heavy Higgses to non-SM "ino" pairs can be significantly large. Moreover, the charginos and neutralinos produced from the decay of heavy Higgses can themselves also undergo long cascade decays depending upon the

[4]In a recent study [75], it has been shown that LHC constraints are significantly weaker in models with Higgsino-dominated $\tilde{\chi}_1^{\pm}$, $\tilde{\chi}_2^0$ and $\tilde{\chi}_3^0$ compared to the scenarios studied by the LHC collaborations with wino-dominated $\tilde{\chi}_1^{\pm}$, $\tilde{\chi}_2^0$.

[5]We do not consider the CMS constraints as we find them comparable with those of the ATLAS Collaboration.

[6]For details about the implementation and validation of our analysis, see Ref. [76].

choice of MSSM parameters. As such, a myriad of possible cascade decay modes are possible corresponding to various final-state topologies. For example, one can have a very simple cascade decay of the form $H \to \tilde{\chi}_2^0\tilde{\chi}_1^0, \tilde{\chi}_2^0 \to Z/h\tilde{\chi}_1^0$, resulting in a mono-$Z/h + \not{E}_T$ final state, or $H^\pm \to \tilde{\chi}_1{}^\pm\tilde{\chi}_1^0$, $\tilde{\chi}_1{}^\pm \to W^\pm\tilde{\chi}_1^0$, resulting in a mono-$W + \not{E}_T$ final state. However, one can also encounter relatively complex cascade decays with multiple decay chains in between, for example, $H \to \tilde{\chi}_2^0\tilde{\chi}_3^0$, $\tilde{\chi}_2^0 \to Z\tilde{\chi}_1^0$, $\tilde{\chi}_3^0 \to W^\pm\tilde{\chi}_1{}^\mp$, which may eventually lead to final states with multiple leptons and jets along with large missing energy. As we have already mentioned, one can have a significant branching fraction for these cascade decays by making judicious choices of the parameters. A proper understanding of these cascade decays with various possible final-state topologies can be considered as a direct probe of the MSSM Higgs sector. In this work, we perform a detailed collider analysis of the MSSM heavy Higgses focusing on the mono-$X + \not{E}_T$ ($X = W,\ Z$) and trilepton $+ \not{E}_T$ channels (where leptons originate from the SM W/Z gauge bosons) in the context of a 14 TeV high-luminosity run of the LHC. Here we assume that the SM gauge bosons W/Z decay leptonically, i.e., $W \to \ell\nu$ and $Z \to \ell\ell$ with $\ell = e, \mu$, in order to reduce the SM backgrounds significantly. The hadronic decay modes might also be important; however, we do not consider them in this work. Searches through mono-Higgs plus $\not{E}_T$ also exist in the literature; for details see Ref. [78].

A. Benchmark points

To present the collider analysis we choose four optimized benchmark points (BP-1 to BP-4) suitable for the above-mentioned three search strategies. All the model parameters, the masses of heavy Higgses and electroweakinos, and the relevant branching ratios are summarized in Table IV. For all four benchmark points, heavy Higgs masses lie in the mass range of 500–700 GeV. The first two benchmark points, BP-1 and BP-2, are optimized for the mono-$Z + \not{E}_T$ searches, where the lightest chargino and the second/third lightest neutralinos are Higgsino dominated and the LSP is bino dominated. In BP-1, $\mathrm{BR}(\tilde{\chi}_2^0, \tilde{\chi}_3^0 \to Z\tilde{\chi}_1^0) = 100\%$ and the total contribution coming from H/A to $\tilde{\chi}_2^0\tilde{\chi}_1^0, \tilde{\chi}_3^0\tilde{\chi}_1^0$ is about 30%, while in BP-2 the decay modes $\tilde{\chi}_2^0$, $\tilde{\chi}_3^0 \to h\tilde{\chi}_1^0$ open up and consequently the branching ratios to $Z\tilde{\chi}_1^0$ get reduced. Our third benchmark point, BP-3, is optimized for the mono-$W + \not{E}_T$ searches where the LSP is a mixture of substantial wino and Higgsino components, while $\tilde{\chi}_2^0, \tilde{\chi}_3^0$ are Higgsino dominated. Here $\tilde{\chi}_1{}^\pm$ is primarily wino but has a significant Higgsino component. In Table IV, all the relevant branching ratios of $H/A \to \chi_1^\pm\chi_2^\mp$, $\tilde{\chi}_1^0\chi_{2,3}^0$ are summarized. In BP-4, the input parameters M_1, M_2, and μ all are relatively light and close to each other, and hence the charginos and neutralinos are mixed states of bino, wino, and Higgsino states. Several possible long cascade decays of these electroweakinos (see last column of Table IV) lead to final-state topologies with trileptons plus missing energy.

In Table V we present the production cross sections of the MSSM heavy Higgses H, A, and $H^\pm$ for center-of-mass energies $\sqrt{s} = 8, 13$, and 14 TeV. From the last row of Table V, it is clear that the charged Higgs production cross sections are much smaller compared to the H, A cross sections, and hence we ignore them in the rest of our analysis. Once we know the cross sections of these Higgses and also the branching ratios to different decay modes, we can calculate the quantity $\sigma \times \mathrm{BR}$ for all the benchmark points and then compare our results with the present experimental bounds. In Table VI, we display the observed 95% C.L. upper limits on the production cross section times branching ratios for the heavy Higgses obtained by the ATLAS and CMS collaborations using the Run-I and Run-II data. We also quote the predictions for a given decay mode associated to all four benchmark points. Here, we consider the following Higgs decay modes: $H/A \to \gamma\gamma$, WW, ZZ, hh, $\tau\tau$; $A \to Zh$; $H^\pm \to \tau\nu$, $t\bar{b}$. The quantity $\sigma \times \mathrm{Br}(H/A \to XX)^{\mathrm{UL}}_{\mathrm{ATLAS/CMS}}$ denotes the 95% C.L. upper limit on the production cross section times branching ratios observed by the ATLAS/CMS collaborations, and $\sigma \times \mathrm{Br}(H/A \to XX)$ is the same but for our representative benchmark points for a generic heavy Higgs decay $H/A \to XX$ channel. We observe that, in most of the cases, the limits from LHC Run-I data are more stringent than the early Run-II data and, except for the $H/A \to \tau\tau$ channel, the observed upper limits are a few orders of magnitude larger than the predicted values for the benchmark points.

In addition to the heavy Higgs direct search bounds, we also consider the limits obtained from the direct searches of the charginos and neutralinos at the LHC. Both the ATLAS and CMS collaborations have searched for these electroweakinos, and placed upper limits on the production cross sections. We find that the limits of the ATLAS and CMS collaborations are comparable, and so in our analysis we use the ATLAS limits only. All the benchmark points, BP-1 to BP-4, posses significant gaugino-Higgsino mixing which leads to sizable modifications in electroweakino pair-production cross sections. We calculate all the dominant chargino-neutralino pair-production cross sections (see Table VII) and then, following the ATLAS analysis [68,71], we estimate the cut efficiencies for the three final-state topologies $3\ell + \not{E}_T$, $1\ell + 2b + \not{E}_T$, and $1\ell + 2\gamma + \not{E}_T$ ($\ell = e,\ \mu$). In Table VII, we present the observed 95% C.L. upper limits on the number of BSM signal events, $N^{\mathrm{Obs\,UL}}_{\mathrm{BSM}}$, by the ATLAS Collaboration for the most sensitive signal regions for the above-mentioned three channels. In Table VII we also present the production cross sections and N_{BSM} for our benchmark points for the 8 TeV LHC with $\mathcal{L} = 20.3\ \mathrm{fb}^{-1}$, where the quantity $N_{\mathrm{BSM}} =$ production cross section $\times$ efficiency $\times$ luminosity for a given channel. From the table, it is evident that the model predictions are much smaller compared to the observed

TABLE IV. Input parameters, masses of heavy Higgses and electroweakinos, and branching fractions of relevant processes for benchmark points. Here all the input mass parameters and output masses are in GeV.

Benchmark Points	Parameters (GeV)	Mass (GeV)	Processes	Branching Fraction
	$M_A = 591.2$, $M_1 = 127.1$,	$M_{\chi_1^0} = 119.7$	$H \to \chi_2^0 \chi_1^0$	4.58%
BP-1	$M_2 = 900$, $\mu = 237.2$,	$M_{\chi_2^0} = 241.8$	$H \to \chi_3^0 \chi_1^0$	10.14%
	$\tan\beta = 15$, $A_t = 1890$,	$M_{\chi_3^0} = 241.8$	$A \to \chi_2^0 \chi_1^0$	9.23%
	$m_{\tilde{Q}_{3l}} = 4160$, $m_{\tilde{t}_R} = 6520$,	$M_{\chi_4^0} = 907.4$	$A \to \chi_3^0 \chi_1^0$	4.65%
	$m_{\tilde{b}_R} = 2280$, $A_b = A_\tau = 0$	$M_{\chi_1^\pm} = 234.3$	$\chi_2^0 \to Z \chi_1^0$	100%
	$M_3 = 2960$	$M_{\chi_2^\pm} = 907.4$	$\chi_3^0 \to Z \chi_1^0$	100%
		$M_H = 591.3$		
		$M_{H^\pm} = 596.8$		
	$M_A = 550$, $M_1 = 80$,	$M_{\chi_1^0} = 77.2$	$H \to \chi_2^0 \chi_1^0$	4.82%
BP-2	$M_2 = 900$, $\mu = 350$,	$M_{\chi_2^0} = 347.8$	$H \to \chi_3^0 \chi_1^0$	13.93%
	$\tan\beta = 8.5$, $A_t = 3770$,	$M_{\chi_3^0} = 353.6$	$A \to \chi_2^0 \chi_1^0$	14.14%
	$m_{\tilde{Q}_{3l}} = 3380$, $m_{\tilde{t}_R} = 9040$,	$M_{\chi_4^0} = 908.5$	$A \to \chi_3^0 \chi_1^0$	3.89%
	$m_{\tilde{b}_R} = 2820$, $A_b = A_\tau = 0$	$M_{\chi_1^\pm} = 345.1$	$\chi_2^0 \to Z \chi_1^0$	24.25%
	$M_3 = 8900$	$M_{\chi_2^\pm} = 908.5$	$\chi_3^0 \to Z \chi_1^0$	83.56%
		$M_H = 550.6$		
		$M_{H^\pm} = 556.0$		
	$M_A = 600$, $M_1 = 950$,	$M_{\chi_1^0} = 158.2$	$H \to \chi_1^\pm \chi_2^\mp$	23.39%
BP-3	$M_2 = 178.2$, $\mu = 286.1$,	$M_{\chi_2^0} = 292.7$	$A \to \chi_1^\pm \chi_2^\mp$	16.70%
	$\tan\beta = 21$, $A_t = 4320$,	$M_{\chi_3^0} = 310.3$	$\chi_2^\pm \to W^\pm \chi_1^0$	43.48%
	$m_{\tilde{Q}_{3l}} = 3370$, $m_{\tilde{t}_R} = 4230$,	$M_{\chi_4^0} = 952.3$	$H \to \chi_1^0 \chi_2^0$	8.30%
	$m_{\tilde{b}_R} = 5330$, $A_b = A_\tau = 0$	$M_{\chi_1^\pm} = 159.0$	$H \to \chi_1^0 \chi_3^0$	1.30%
	$M_3 = 7100$	$M_{\chi_2^\pm} = 316.8$	$A \to \chi_1^0 \chi_2^0$	3.05%
		$M_H = 600.0$	$A \to \chi_1^0 \chi_3^0$	4.10%
		$M_{H^\pm} = 605.5$	$\chi_2^0 \to \chi_1^\pm W^\mp$	73.32%
			$\chi_3^0 \to \chi_1^\pm W^\mp$	81.06%
	$M_A = 657.5$, $M_1 = 159.5$,	$M_{\chi_1^0} = 145.5$	$H \to \chi_1^\pm \chi_2^\mp$	28.971%
BP-4	$M_2 = 337.2$, $\mu = 236.6$,	$M_{\chi_2^0} = 230.7$	$A \to \chi_1^\pm \chi_2^\mp$	15.8%
	$\tan\beta = 23$, $A_t = 1290$,	$M_{\chi_3^0} = 248.9$	$\chi_2^\pm \to W^\pm \chi_3^0$	21.85%
	$m_{\tilde{Q}_{3l}} = 9590$, $m_{\tilde{t}_R} = 1920$,	$M_{\chi_4^0} = 387.6$	$\chi_3^0 \to Z \chi_1^0$	100%
	$m_{\tilde{b}_R} = 2600$, $A_b = A_\tau = 0$	$M_{\chi_1^\pm} = 221.4$	$H \to \chi_3^0 \chi_4^0$	8.89%
	$M_3 = 6180$	$M_{\chi_2^\pm} = 387.3$	$A \to \chi_3^0 \chi_4^0$	0.39%
		$M_H = 657.5$	$\chi_4^0 \to W^\pm \chi_1^\pm$	67.78%
		$M_{H^\pm} = 662.4$		

TABLE V. Production cross sections of the heavy Higgses H, A, and $H^\pm$ for $\sqrt{s} = 8, 13$, and 14 TeV. The Higgses are produced through ggF and bbF processes. Charged Higgs production cross sections are small, so we ignore them in our analysis.

	Production cross section in fb							
	8 TeV				13(14) TeV			
	BP-1	BP-2	BP-3	BP-4	BP-1	BP-2	BP-3	BP-4
H	65	41	114	21	290(356)	171(207)	517(635)	100(129)
A	70	51	119	24	311(380)	208(252)	534(657)	114(140)
$H^\pm$	1.1	0.8	1.9	0.4	7.3(9.4)	5.12(6.5)	12.9(16.8)	3.2(4.2)

TABLE VI. Upper limits on the production cross section times the branching ratios at 95% C.L. for various decay modes obtained by the ATLAS and CMS collaborations and the corresponding values for the benchmark points introduced in Table IV.

	$\sqrt{s} = 8$ TeV (fb)				$\sqrt{s} = 13$ TeV (fb)			
Modes	BP-1	BP-2	BP-3	BP-4	BP-1	BP-2	BP-3	BP-4
$\sigma \times \mathrm{Br}(H/A \to \gamma\gamma)^{\mathrm{UL}}_{\mathrm{ATLAS}}$ [11,57]	0.9	1.8	0.6	…	3.0	3.6	3.3	2.0
$\sigma \times \mathrm{Br}(H/A \to \gamma\gamma)^{\mathrm{UL}}_{\mathrm{CMS}}$ [12,58]	1.4	1.2	1.0	0.5	5.1	4.6	3.7	1.3
$\sigma \times \mathrm{Br}(H/A \to \gamma\gamma)$	$\sim 10^{-6}$	$\sim 10^{-4}$	$\sim 10^{-4}$	$\sim 10^{-6}$	$\sim 10^{-4}$	$\sim 10^{-3}$	$\sim 10^{-3}$	$\sim 10^{-4}$
$\sigma \times \mathrm{Br}(H \to WW)^{\mathrm{UL}}_{\mathrm{ATLAS}}$ [13,61]	242.8	308.6	229.3	186.5	570.7	817.7	543.2	457.8
$\sigma \times \mathrm{Br}(H \to WW)^{\mathrm{UL}}_{\mathrm{CMS}}$ [14]	124.99	148.02	121.28	109.65	…	…	…	…
$\sigma \times \mathrm{Br}(H \to WW)$	0.04	0.18	0.01	0.01	0.18	0.76	0.06	0.06
$\sigma_{ggH} \times \mathrm{Br}(H \to ZZ)^{\mathrm{UL}}_{\mathrm{ATLAS}}$ [15,62]	23.7	30.8	21.2	26.2	329.8	456.4	304.1	195.8
$\sigma_{ggH} \times \mathrm{Br}(H \to ZZ)$	$\sim 10^{-3}$	0.02	$\sim 10^{-4}$	$\sim 10^{-5}$	$\sim 10^{-3}$	0.11	$\sim 10^{-3}$	$\sim 10^{-3}$
$\sigma \times \mathrm{Br}(H \to ZZ)^{\mathrm{UL}}_{\mathrm{CMS}}$ [14]	128.96	140.01	125.32	117.71	…	…	…	…
$\sigma \times \mathrm{Br}(H \to ZZ)$	0.02	0.09	$\sim 10^{-2}$	$\sim 10^{-3}$	0.09	0.37	0.03	0.03
$\sigma_{ggH} \times \mathrm{Br}(H \to hh)^{\mathrm{UL}}_{\mathrm{ATLAS}}$ [20]	87.8	121.1	79.1	42.3	…	…	…	…
$\sigma_{ggH} \times \mathrm{Br}(H \to hh)$	0.01	0.2	0.002	0.006	0.04	0.78	0.009	0.024
$\sigma \times \mathrm{Br}(H \to hh \to \gamma\gamma b\bar{b})^{\mathrm{UL}}_{\mathrm{CMS}}$ [19]	1.19	1.47	1.13	0.77	…	…	…	…
$\sigma \times \mathrm{Br}(H \to hh \to \gamma\gamma b\bar{b})$	$\sim 10^{-4}$	$\sim 10^{-4}$	$\sim 10^{-4}$	$\sim 10^{-4}$	$\sim 10^{-3}$	$\sim 10^{-3}$	$\sim 10^{-3}$	$\sim 10^{-4}$
$\sigma_{gg\phi} \times \mathrm{Br}(\phi \to \tau\tau)^{\mathrm{UL}}_{\mathrm{ATLAS}}$ [24,65]	19.1	21.9	19.0	15.6	112.0	148.3	104.1	83.8
$\sigma_{gg\phi} \times \mathrm{Br}(\phi \to \tau\tau)^{\mathrm{UL}}_{\mathrm{CMS}}$ [23,64]	23.1	29.6	22.4	17.5	85.7	96.5	84.6	75.2
$\sigma_{ggH+ggA} \times \mathrm{Br}(H/A \to \tau\tau)$	1.46	2.24	1.14	0.31	5.62	8.38	4.44	1.29
$\sigma_{bb\phi} \times \mathrm{Br}(\phi \to \tau\tau)^{\mathrm{UL}}_{\mathrm{ATLAS}}$ [24,65]	19.1	21.9	18.6	14.9	106.7	147.8	97.6	80.1
$\sigma_{bb\phi} \times \mathrm{Br}(\phi \to \tau\tau)^{\mathrm{UL}}_{\mathrm{CMS}}$ [23,64]	22.7	25.7	21.4	20.2	72.8	79.0	71.1	93.4
$\sigma_{bbH+bbA} \times \mathrm{Br}(H/A \to \tau\tau)$	11.62	3.51	14.97	1.30	52.46	15.15	68.28	6.35
$\sigma \times \mathrm{Br}(A \to Zh)^{\mathrm{UL}}_{\mathrm{ATLAS}}$ [21,66]	41.4	43.1	41.0	26.3	412.6	709.9	365.3	250.3
$\sigma \times \mathrm{Br}(A \to Zh)^{\mathrm{UL}}_{\mathrm{CMS}}$ [22]	83.29	131.9	67.0	…	…	…	…	…
$\sigma \times \mathrm{Br}(A \to Zh)$	0.04	0.2	0.013	0.0062	0.16	0.8	0.06	0.03
$\sigma \times \mathrm{Br}(H^{\pm} \to \tau\nu)^{\mathrm{UL}}_{\mathrm{ATLAS}}$ [28,67]	11.12	14.48	9.94	8.84	53.4	66.9	50.3	39.2
$\sigma \times \mathrm{Br}(H^{\pm} \to \tau\nu)^{\mathrm{UL}}_{\mathrm{CMS}}$ [26]	26.28	30.31	25.97	…	…	…	…	…
$\sigma \times \mathrm{Br}(H^{\pm} \to \tau\nu)$	0.12	0.05	0.14	0.02	0.76	0.33	0.96	0.12
$\sigma \times \mathrm{Br}(H^{\pm} \to t\bar{b})^{\mathrm{UL}}_{\mathrm{ATLAS}}$ [29]	208.7	487.7	238.8	…	…	…	…	…
$\sigma \times \mathrm{Br}(H^{\pm} \to t\bar{b})^{\mathrm{UL}}_{\mathrm{CMS}}$ [26]	137.1	166.1	132.7	…	…	…	…	…
$\sigma \times \mathrm{Br}(H^{\pm} \to t\bar{b})$	0.78	0.59	0.89	0.13	5.09	3.69	5.90	0.99

TABLE VII. Here the cross sections (NLO) are in fb. $N^{\mathrm{Obs\,UL}}_{\mathrm{BSM}}$ stands for observed upper limits on N_{BSM} at 95% C.L., where $N_{\mathrm{BSM}} =$ production cross section $\times$ efficiency $\times$ luminosity.

	BP-1	BP-2	BP-3	BP-4
$\sigma(pp \to \tilde{\chi}_1^{\pm}\tilde{\chi}_2^0)$	91.01	18.76	17.75	131.24
$\sigma(pp \to \tilde{\chi}_1^{\pm}\tilde{\chi}_3^0)$	95.57	17.77	13.12	85.55
$\sigma(pp \to \tilde{\chi}_1^{\pm}\tilde{\chi}_4^0)$	…	…	…	3.32
$\sigma(pp \to \tilde{\chi}_2^{\pm}\tilde{\chi}_2^0)$	…	…	29.35	3.61
$\sigma(pp \to \tilde{\chi}_2^{\pm}\tilde{\chi}_3^0)$	…	…	39.39	3.93
$\sigma(pp \to \tilde{\chi}_2^{\pm}\tilde{\chi}_4^0)$	…	…	…	35.07
σ_{Total}	187.6	36.53	99.61	262.68
N_{BSM} for SR0τa-bin16 ($N^{\mathrm{Obs\,UL}}_{\mathrm{BSM}} = 5.2$ [68])	0.93	0.99	0.48	0.65
N_{BSM} for SRlbb-2 ($N^{\mathrm{Obs\,UL}}_{\mathrm{BSM}} = 5.5$ [71])	0	0.76	0.1	0.05
N_{BSM} for SR$l\gamma\gamma$-1 ($N^{\mathrm{Obs\,UL}}_{\mathrm{BSM}} = 3.6$ [71])	0	0.08	0.05	0.02

95% C.L. upper limits, and thus all our benchmark points are consistent with the updated bounds associated to direct searches of the electroweakinos at the LHC.

B. Mono-X plus missing energy

Events with a single W/Z boson plus missing transverse energy ($\not{E}_T$) constitute a very clean and distinctive signature in new physics searches at the LHC. This topology has been thoroughly analyzed by both the ATLAS and CMS collaborations, mainly in the context of dark matter (DM) searches. In this paper, we consider two such mono-$X + \not{E}_T$ channels, namely mono-Z and mono-W, with both W, Z decaying leptonically ($Z \to ll$, $W \to l\nu$, $l = e, \mu$) to search for the MSSM heavy Higgses at the LHC.

Below, we discuss the details of the collider analysis for our optimized benchmark points for the above-mentioned mono-X search channels. We use MADGRAPH (version 2.3.3) [79] to generate the background events and PYTHIA (version 6.428) [80] for showering and hadronization. The production cross sections of the heavy Higgses H, A have been calculated using SUSHI (version 1.5.0) [81], while for the charged Higgs boson $H^{\pm}$ we use PYTHIA. To obtain the particle spectrum we use SUSPECT, while SUSYHIT has been used to calculate the Higgs and SUSY decay widths and branching ratios. The signal events have been generated through the gluon-gluon fusion process using PYTHIA. Both the signal and background events have been passed through a fast detector simulation using DELPHES3 (version-3.3.2) [82] using the default ATLAS card.

1. Mono-Z(leptonic) + $\not{E}_T$ channel

We perform a search for the MSSM heavy Higgses in events with a leptonically decaying Z boson ($Z \to \ell^+\ell^-$, $\ell = e, \mu$) produced through cascade decays of the charginos and neutralinos in the context of the $\sqrt{s} = 14$ TeV run of the LHC with an integrated luminosity of 3000 fb^{-1}. These events also contain significant missing transverse energy coming from the lightest neutralinos. The search strategy reported in Ref. [83], which focused on the DM searches, has been followed with suitable modifications aimed to optimize the signal significance. This analysis has been performed on the first two representative benchmark points, BP-1 and BP-2 (see Table IV). The relevant decay chains giving rise to the above-mentioned final-state signature are $pp \to H/A$, $H/A \to \tilde{\chi}^0_{2,3}\tilde{\chi}^0_1$, and $\tilde{\chi}^0_{2,3} \to \tilde{\chi}^0_1 Z$.

The events are selected with two same-flavor opposite-sign (SFOS) isolated leptons (electrons or muons) with p_T greater than 20 GeV. Candidate electrons (muons) are required to be within the pseudorapidity range $|\eta| < 2.47(2.5)$. For an electron or muon to be isolated, the scalar p_T sum of all stable particles with $p_T > 1$ GeV present within a cone of radius $\Delta R = 0.2$ around the direction of the candidate lepton should be less than 10% of the p_T of the candidate lepton, where $\Delta R = \sqrt{(\Delta\phi)^2 + (\Delta\eta)^2}$ with ϕ being the azimuthal angle. The azimuthal angle between the dilepton system and the $\not{E}_T$ direction, $\Delta\phi_{p_T^{\ell\ell},\not{E}_T}$, is required to be greater than 2.5, where $p_T^{\ell\ell}$ is the momentum of the dilepton system. In addition, the absolute value of the pseudorapidity of the dilepton system, $|\eta_{\ell\ell}|$, must lie within 2.5 and the invariant mass of the SFOS pair is required to be within $M_Z \pm 15$ GeV, where M_Z is the Z boson mass. Events with one or more jets with p_T greater than 25 GeV are rejected. To further reduce the SM backgrounds, we define a kinematic variable ξ constructed using the dilepton p_T and $\not{E}_T$ as $|p_T^{\ell\ell} - \not{E}_T|/p_T^{\ell\ell}$, where $\ell = e, \mu$.

TABLE VIII. Signal regions SRA1 and SRB1 defined using the missing energy ($\not{E}_T$) and transverse momentum of the dilepton system where we define $\xi = \frac{|p_T^{\ell\ell} - \not{p}_T|}{p_T^{\ell\ell}}$.

Signal Regions	Selection Cuts
SRA1	$\not{p}_T > 125$ GeV and $\xi < 0.3$
SRB1	$\not{p}_T > 150$ GeV and $\xi < 0.5$

TABLE IX. Number of signal and background events at the 14 TeV run of the LHC with 3000 fb^{-1} of luminosity obtained after the imposition of our selection cuts for the mono-$Z + \not{p}_T$ channel. Here we focus on the first two representative benchmark points BP-1 and BP-2.

Signal	Signal		Backgrounds		Significance	
Regions	BP-1	BP-2	ZZ	WZ	BP-1	BP-2
SRA1	921	804	15077	5738	7.45	6.50
SRB1	506	619	9187	3152	5.24	6.41

The dominant SM background, which is also an irreducible background, is $pp \to ZZ \to \ell^+\ell^-\nu\bar{\nu}(\ell = e, \mu)$. However, processes like $pp \to W^+W^- \to \ell^+\nu\ell^-\bar{\nu}$, $WZ \to \ell\nu\ell^+\ell^-$, and $ZZ \to \ell^+\ell^-\ell^+\ell^-$ also contribute to the SM backgrounds when additional leptons get misidentified or remain unreconstructed. Two signal regions, SRA1 and SRB1, are constructed using specific choices of cuts on $\not{E}_T$ and ξ; see Table VIII. The signal region SRB1 is motivated from the ATLAS analysis [83] where $\not{E}_T$ is large. The signal region SRA1 is based on our reoptimization of the signal significances with relatively smaller values of $\not{E}_T$ and ξ. The number of signal and background events corresponding to each signal region are shown in Table IX. For both SRA1 and SRB1, we find that one can obtain 5σ statistical significance at the 14 TeV LHC with 3000 fb^{-1} of luminosity. Here statistical significance has been calculated as $S/\sqrt{B}$ where S (B) is the number of signal (background) events. We would like to point out that we have not taken into account the direct neutralino pair-production cross sections in the calculation of signal significances. Adding up the $\tilde{\chi}^0_1\tilde{\chi}^0_2$ and $\tilde{\chi}^0_1\tilde{\chi}^0_3$ direct production processes will lead to a $\approx$27% ($\approx$4%) increase in the signal yield for BP-1 (BP-2). The signal significances will attain values of 9.31 (6.55) and 6.76 (6.67) in SRA1 (SRB1) corresponding to BP-1 and BP-2, respectively.

Here we would like to mention that in order to perform this search, the lower limits on the $\not{E}_T$ selection cuts need to be restricted to relatively lower values (<200 GeV) as the signal yield becomes statistically insignificant in the higher-$\not{E}_T$ regime. The results of this analysis indicate a possibility to marginally discover/exclude the heavy Higgses at a high-luminosity LHC run. However, we would like to mention here that the signal significances have been calculated assuming zero systematic uncertainty. As the systematic uncertainty comes into play, the signal significance will get significantly reduced and will go down much below the 5σ discovery limit.

2. Mono-(leptonic) + $\not{E}_T$ channel

Here we present a search strategy for MSSM heavy Higgs bosons in events with a leptonically decaying W

boson ($W \to \ell\nu$, $\ell = e, \mu$) and significant missing transverse energy for the $\sqrt{s} = 14$ TeV run of the LHC with an integrated luminosity of $3000\ \mathrm{fb}^{-1}$. The W boson is produced through cascade decay of heavy Higgses, which first decays to a pair of neutralinos and/or charginos which then undergo further decay, generating final states containing a W boson and large missing transverse energy. These events generally contain relatively soft leptons or jets. Here we follow the collider strategy as reported in Ref. [84]; however, some changes have been implemented in order to optimize the signal significances. The representative benchmark point BP-3 has been used to perform the detailed analysis. The decay chains of BP-3 relevant for this analysis are given below:

$$pp \to H/A \to \tilde{\chi}_1^{\pm}\tilde{\chi}_2^{\mp}, \qquad \tilde{\chi}_2^{\mp} \to W^{\mp}\tilde{\chi}_1^0,$$
$$pp \to H/A \to \tilde{\chi}_1^0\tilde{\chi}_{2,3}^0, \qquad \tilde{\chi}_{2,3}^0 \to W^{\pm}\tilde{\chi}_1^{\mp}.$$

From Table IV, it can be seen that for BP-3, $\tilde{\chi}_1^0$ and $\tilde{\chi}_1^{\pm}$ are almost degenerate in mass; as a result, $\tilde{\chi}_1^{\pm}$ undergoes three-body decays resulting in soft leptons or jets in the final state. Similarly, the cascade decay chain originating from $H^{\pm}$ can also lead to a mono-$W + \not{E}_T$ signature. However, we have not considered these decay chains in our analysis because of the relatively smaller production cross sections of $H^{\pm}$.

The candidate events are required to have exactly one isolated electron or muon in the final state with $p_T > 30$ GeV. The candidate electron (muon) is required to satisfy $|\eta| < 2.47(2.50)$. The isolation criteria for the candidate leptons is exactly same as what we discussed in the last section. In addition, events are rejected if they contain one or more jets with $p_T > 25$ GeV. For final-state topologies with one isolated lepton and missing energy, we usually define a kinematic observable called the transverse mass M_T defined using the four-momenta of the lepton and $\not{E}_T$ as

$$M_T = \sqrt{2|p_T^{\ell}|\not{E}_T(1 - \cos(\Delta\Phi_{\ell,\not{p}_T}))},$$

where $\Delta\Phi_{\ell,\not{p}_T}$ is the azimuthal angle between the candidate lepton and the $\not{p}_T$ direction. The dominant source of SM background is the $pp \to \ell\nu j$ production channel which has been generated with a transverse mass cut $M_T^{\ell\nu} > 100$ GeV, where $M_T^{\ell\nu}$ is the transverse mass of the lepton neutrino pair. Besides, processes like diboson production, $t\bar{t}$, etc., also contribute significantly to the background list. Among the diboson modes, the dominant contribution comes from the $\mathrm{WZ} \to \ell\nu\nu\bar{\nu}$ and $\mathrm{WW} \to \ell\nu\ell\nu$ ($\ell = e, \mu$) channels.

TABLE X. Signal regions for the mono-$W + \not{E}_T$ analysis. The transverse mass (M_T) is defined using the four-momenta of the lepton and the missing transverse momentum $\not{E}_T$.

Signal Regions	Selection Cuts
SRA2	$\not{E}_T > 50$ GeV and $M_T > 175$ GeV
SRB2	$\not{E}_T > 100$ GeV and $M_T > 125$ GeV

Similar to the earlier analysis, two signal regions—SRA2 and SRB2—with different optimized values of $\not{E}_T$ and M_T are constructed, as displayed in Table X. For both signal regions SRA2 and SRB2, we further select those leptons which satisfy $|\eta^{\ell}| < 1.5$, with $\ell = e, \mu$. The choice of these signal regions is driven from the optimization of the signal significances. We investigate several combinations of selection variables $\not{E}_T$ and M_T, and among them, two signal regions (SRA2 and SRB2) are chosen which yield the most efficient optimization of signal significances. The expected number of signal and background events at the 14 TeV run of the LHC with $3000\ \mathrm{fb}^{-1}$ of luminosity are shown in Table XI for both of the above-mentioned signal regions. Similar to our previous analysis, one needs to restrict the lower bounds on $\not{E}_T$ to 150 GeV as the signal yields become relatively insignificant as one shifts towards the high-$\not{E}_T$ regime. Here again, we calculate the statistical significance using the signal and background events, and find that it is around 2σ with $3000\ \mathrm{fb}^{-1}$ of luminosity at the 14 TeV run of the LHC. This indicates that it would be very difficult to discover/exclude the heavy Higgs through this channel. More efficient signal optimizations and more precise understanding of the backgrounds may be required to make this search channel more efficient. However, we would like to mention that the direct electroweakino pair-production processes have not been considered in the calculation of signal significances. We check that the $\tilde{\chi}_1^{\pm}\tilde{\chi}_2^{\mp}$, $\tilde{\chi}_1^0\tilde{\chi}_2^0$, and $\tilde{\chi}_1^0\tilde{\chi}_3^0$ direct production processes can lead to an $\approx 18\%$ increase in the signal yield. As a result, the signal significance goes to 2.42 (2.44) in SRA2 (SRB2) upon adding the contributions from the relevant direct production processes.

TABLE XI. Number of signal and background events at the 14 TeV run of the LHC with $3000\ \mathrm{fb}^{-1}$ of luminosity obtained after the imposition of our selection cuts for the mono-$W + \not{E}_T$ channel. Here we focus on the third representative benchmark point BP-3.

Signal	Signal	Backgrounds					Significance
Regions	BP-3	$l\nu$	WW	WZ	$t\bar{t}$	ZZ	BP-3
SRA2	6572	1.0×10^7	76427	68426	58204	9088	2.05
SRB2	5499	6.8×10^6	47603	52266	59380	8071	2.07

C. *Trilepton* + $\not{E}_T$ *channel*

In this section, we present a search strategy for the heavy Higgses H, A, $H^\pm$ in events with leptonically decaying W and Z bosons ($W \to \ell\nu$, $Z \to \ell\ell$, $\ell = e, \mu$) produced through cascade decay of heavy Higgses with significant missing transverse energy at the $\sqrt{s} = 14$ TeV run of the LHC with an integrated luminosity of 3000 fb^{-1}. Here we follow the collider strategy reported in Ref. [85], and consider the representative benchmark point BP-4. The relevant decay chains which generate the above-mentioned signature are given below:

$$pp \to H/A, \qquad H/A \to \tilde{\chi}_1^\pm \tilde{\chi}_2^\mp, \qquad \tilde{\chi}_2^\mp \to W^\mp \tilde{\chi}_3^0,$$
$$\tilde{\chi}_3^0 \to Z\tilde{\chi}_1^0, \qquad pp \to H/A, \qquad H/A \to \tilde{\chi}_3^0\tilde{\chi}_4^0,$$
$$\tilde{\chi}_3^0 \to Z\tilde{\chi}_1^0, \qquad \tilde{\chi}_4^0 \to W^\pm \tilde{\chi}_1^\mp.$$

In BP-4, $\tilde{\chi}_1^\pm$ undergoes only three-body decay, resulting in additional leptons or jets in the final state. The cascade decay chain originating from a charged Higgs, with subsequent decays to a chargino-neutralino pair, followed by the decay of charginos and neutralinos to W boson + $\not{E}_T$ and Z boson + $\not{E}_T$, respectively, gains a significant branching fraction and leads to a trilepton plus $\not{E}_T$ signature. However, because of the low production cross section of $H^\pm$, the resultant contribution of these decay modes to the trilepton signatures is relatively low. As a result, similar to previous analyses, we have not taken into account the charged Higgs cascade decay chains in our analysis.

The event selection criteria are almost similar to our previous analyses. Candidate events are required to have exactly three isolated leptons (electron/muon) with $p_T > 20$ GeV. The electrons (muons) are required to lie within $|\eta| < 2.47(2.5)$. Isolation criteria discussed in the previous section apply here as well. Among the three candidate leptons, there must be at least one SFOS pair with invariant mass in the range $|M_Z \pm 15|$ GeV. If there is more than one SFOS pair satisfying the previous condition, then the lepton pair with invariant mass closest to the Z-boson mass is finally identified as the SFOS pair. The transverse mass M_T is defined with respect to the lepton which is not a part of the SFOS pair.

The SM backgrounds for this search channel are $WZ \to \ell\nu\ell\ell$ and $ZZ \to 4\ell$ processes. Here also, we define two signal regions—SRA3 and SRB3—for different conditions of $\not{E}_T$ and M_T, as displayed in Table XII. The choice of signal regions is motivated by the optimization of signal efficiencies as well as the experimental analysis. The number of signal and background events expected at the 14 TeV run of the LHC with 3000 fb^{-1} of luminosity are listed in Table XIII. The estimated statistical significances are very small in this search channel, which indicates that probing the MSSM heavy Higgses through the trilepton + $\not{E}_T$ channel, with leptons originating from the cascade decays of the heavy Higgses, would be an extremely challenging task even at the 14 TeV run of the LHC. Here again, the direct production processes for the relevant chargino and neutralino pairs have not been taken into account while calculating the signal significances. The relevant direct pair-production processes here are $\tilde{\chi}_1^\pm \tilde{\chi}_2^\mp$ and $\tilde{\chi}_3^0\tilde{\chi}_4^0$, and adding them up can lead to a ≈25% increase in signal yield. Thus, the signal significance attains a value of 0.36 (0.27) in SRC1 (SRC2) after adding these direct production processes.

TABLE XII. Signal regions for the $3l + \not{E}_T$ analysis. The transverse mass (M_T) is defined using the four-momenta of the lepton not forming the SFOS pair and the missing transverse momentum $\not{E}_T$.

Signal Regions	Selection Cuts
SRA2	$\not{E}_T > 50$ GeV and $M_T > 150$ GeV
SRB2	$\not{E}_T > 50$ GeV and $M_T > 200$ GeV

TABLE XIII. Number of signal and background events at the 14 TeV run of the LHC with 3000 fb^{-1} of luminosity obtained after the imposition of our selection cuts for the $3l + \not{E}_T$ channel. Here we focus on the fourth representative benchmark point BP-4.

Signal Regions	Signal BP-4	Backgrounds WZ	ZZ	Significance BP-4
SRA3	6.92	544	21	0.29
SRB3	4.33	389	16	0.22

IV. SUMMARY

Precise measurements of the properties of the discovered Higgs boson have been one of the major goals of the LHC physics program. So far, LHC 7 and 8 TeV data reveals that the properties of this new particle are consistent with the SM Higgs boson within the uncertainty in Higgs couplings measurements. Many new physics models beyond the SM contain additional Higgs doublets leading to additional Higgses. A multitude of searches have been performed by the ATLAS and CMS collaborations to probe the heavy Higgses (H, A, and $H^\pm$) of the MSSM through their decay to the SM particles. Note that so far none of these searches have provided a clear signature of the heavier Higgs states. In this regard, it becomes important to examine the non-SM decay modes of the heavier Higgses. The primary motivation for performing such analyses is that when these heavy Higgses decay to light SUSY particles, all the branching ratios to SM particles acquire significant modifications, which changes the whole framework of the LHC search strategy. Moreover, there exist certain regions of the parameter space with intermediate $\tan\beta$ (~5–15), where the heavy Higgs couplings to the SM particles become small. However, in this region of interest, one can obtain an appreciable amount of non-SM decays which can be studied at the LHC. One such non-SM decay mode could be the decay of the heavy Higgses to the light electroweakinos (charginos and neutralinos). The study of these non-SM decay modes in the light of updated LHC data is precisely the goal of this paper.

In the presence of light SUSY particles, and if kinematically allowed, these heavy Higgs bosons can decay to SUSY particles with a significantly high branching fraction. In order to estimate these non-SM decays, we started with a simple-minded scan that made the sparticle sector sufficiently heavy except for the electroweakinos—which we assumed are sufficiently light such that Higgs decay is kinematically allowed—and varied $\tan\beta$ over a wide range. From this simple analysis, we found that these non-SM "ino" decays can be as large as 70–80% for relatively low values (~5–10) of $\tan\beta$. However, here we did not impose the updated LHC Higgs data and also other low-energy flavor data. So, in order to perform a detailed analysis, we scanned the MSSM parameter space with the parameters relevant to the electroweakinos, namely, M_1, M_2, μ and, $\tan\beta$, keeping the sleptons and squarks fixed at high scale. All the scanned points were required to have the lightest Higgs boson mass in the range 122 to 128 GeV. We also considered the constraints from the Higgs couplings measurements, where we used the 95% C.L. contours obtained from a global fit analysis performed by the ATLAS and CMS collaborations. In addition, updated bounds from low-energy flavor data in terms of rare b decays $\mathrm{BR}(b \to s\gamma)$ and $\mathrm{BR}(B_s \to \mu^+\mu^-)$ were also considered in our analysis. Now, depending on the values and hierarchy of the electroweakino parameters, we constructed ten representative models (Model-B to Model-BWH), and then estimated various non-SM "ino" decay modes of the heavy Higgs bosons. From the scan, we observed that some of these ino-modes can be as large as 35–40% even after satisfying the updated LHC data. These non-SM decay modes crucially depend on the gaugino-Higgsino mixing, or precisely on the composition of these electroweakino states. However, as we have already mentioned, both the ATLAS and CMS collaborations have searched for additional Higgses at the LHC and put bounds on masses and couplings of these heavy Higgses. So our next task was then to check whether these heavy Higgses, whose non-SM decay modes we are calculating, are still allowed by the current data. Moreover, we also needed to perform consistency checks of these light electroweakinos with the LHC direct search bounds on their masses and couplings obtained at the end of Run-I. Instead of implementing the current bounds from the direct searches of the heavy Higgses and electroweakinos on each point corresponding to our scanned data set, we chose four representative benchmark points, making sure that all these points satisfy the current LHC Run-I and Run-II data.

Once we selected the benchmark points consistent with the present LHC data, we asked the simple question, can we utilize the large branching ratios of the heavy Higgses to electroweakinos and look for collider signatures of the same through cascade decay at the 14 TeV high-luminosity run of the LHC? So, we performed a dedicated collider analysis at $\sqrt{s} = 14$ TeV corresponding to an integrated luminosity of 3000 fb^{-1}. We focused on the leptonic modes of the cascade decays as these channels are very clean at the LHC's busy environment, and also we have better control over the backgrounds. Our collider analysis can be divided into two parts: one focusing on the mono-X plus missing energy signatures (where X represents W or Z bosons,) and another using the trileptonic channel with a significant amount of missing energy. Among the four representative benchmark points, BP-1 and BP-2 were focused to probe the H, A through the mono-$Z + \not{E}_{\mathrm{T}}$ signature, while BP-3 and BP-4 were used to study the heavy Higgses through the mono-$W + \not{E}_{\mathrm{T}}$ and trilepton $+$ $\not{E}_{\mathrm{T}}$ signatures, respectively. Following an ATLAS study and making suitable changes in the selection cuts, we found that the mono-Z channel has the best sensitivity to probe these heavy Higgses, while the other two modes posses mild sensitivity for the exclusion of these additional Higgses at the 14 TeV run of the LHC with 3000 fb^{-1} of luminosity.

Before we end, we would like to note a few important issues. In this work, we focused on the decay of the heavy MSSM Higgses to the light electroweakinos, only setting other SUSY particles decoupled from the spectrum. However, in principle, some of these sparticles (say, top squarks, tau sleptons, etc.) can also be light, and therefore those decay modes will also contribute to the non-SM decay of the heavy Higgses. Moreover, in our collider analysis we restricted ourselves within the leptonic modes only; however, a plethora of final states involving leptons and jets are possible. Furthermore, some of the final-state particles (say, W, Z, or Higgs bosons) can acquire large transverse momenta; in that situation one needs to invoke the state-of-the-art jet substructure techniques to improve the sensitivity of these heavy resonance searches. All of these points are beyond the scope of the current paper; we leave these issues for a future correspondence focusing on the high-luminosity runs of the LHC.

ACKNOWLEDGMENTS

The work of B. B. is supported by the Department of Science and Technology, Government of India under the Grant Agreement No. IFA13-PH-75 (INSPIRE Faculty Award). The work of A. C. is supported by the Lancaster-Manchester-Sheffield Consortium for Fundamental Physics under STFC Grant No. ST/L000520/1.

APPENDIX: HIGGS SIGNAL STRENGTH CONTOURS

At the end of Run-I of the LHC, both the ATLAS and CMS collaborations published the combined 7 and 8 TeV Higgs data [3–5]. The Higgs data has been analyzed assuming that the Higgs is produced via gluon-gluon fusion, vector-boson fusion, associated production with a W/Z boson, and associated production with a pair of top quarks, while it decays through $\gamma\gamma$, WW^*, ZZ^*, $b\bar{b}$, and $\tau^+\tau^-$ final states. As we have already mentioned, these results are generally expressed in terms of the signal strength variables (μ) [as defined in Eq. (9)]. The LHC collaborations have derived limits on the individual as well as two-dimensional planes of these signal strength variables. The 95% C.L. contours in the $\mu^f_{ggF+t\bar{t}h}$, $\mu^f_{\mathrm{VBF+VH}}$ plane have been obtained through a ten-parameter fit corresponding to the five decay modes of the Higgs boson, with "f" being a generic final-state topology [3]. In Fig. 9 (for Model-BH) and Fig. 10 (for Model-BWH), we display those 95% C.L. exclusion contours and overlay our scanned data set for two representative models: Model-BH and Model-BWH. The green points which actually lie within the above-mentioned contours are henceforth accepted for further analysis.

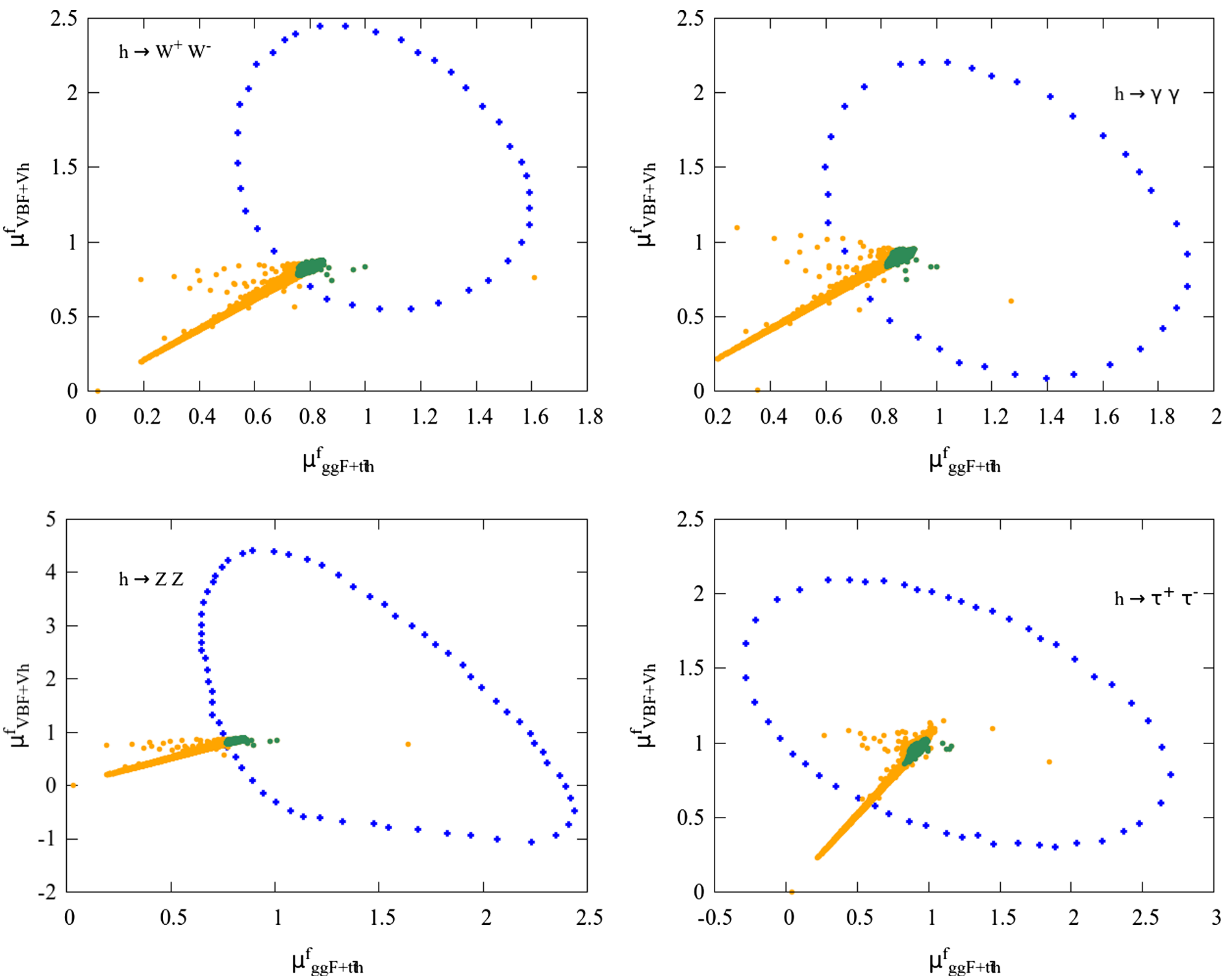

FIG. 9. The 95% C.L. contours in the $\mu^f_{ggF+t\bar{t}h} - \mu^f_{\mathrm{VBF+VH}}$ plane for Model-BH.

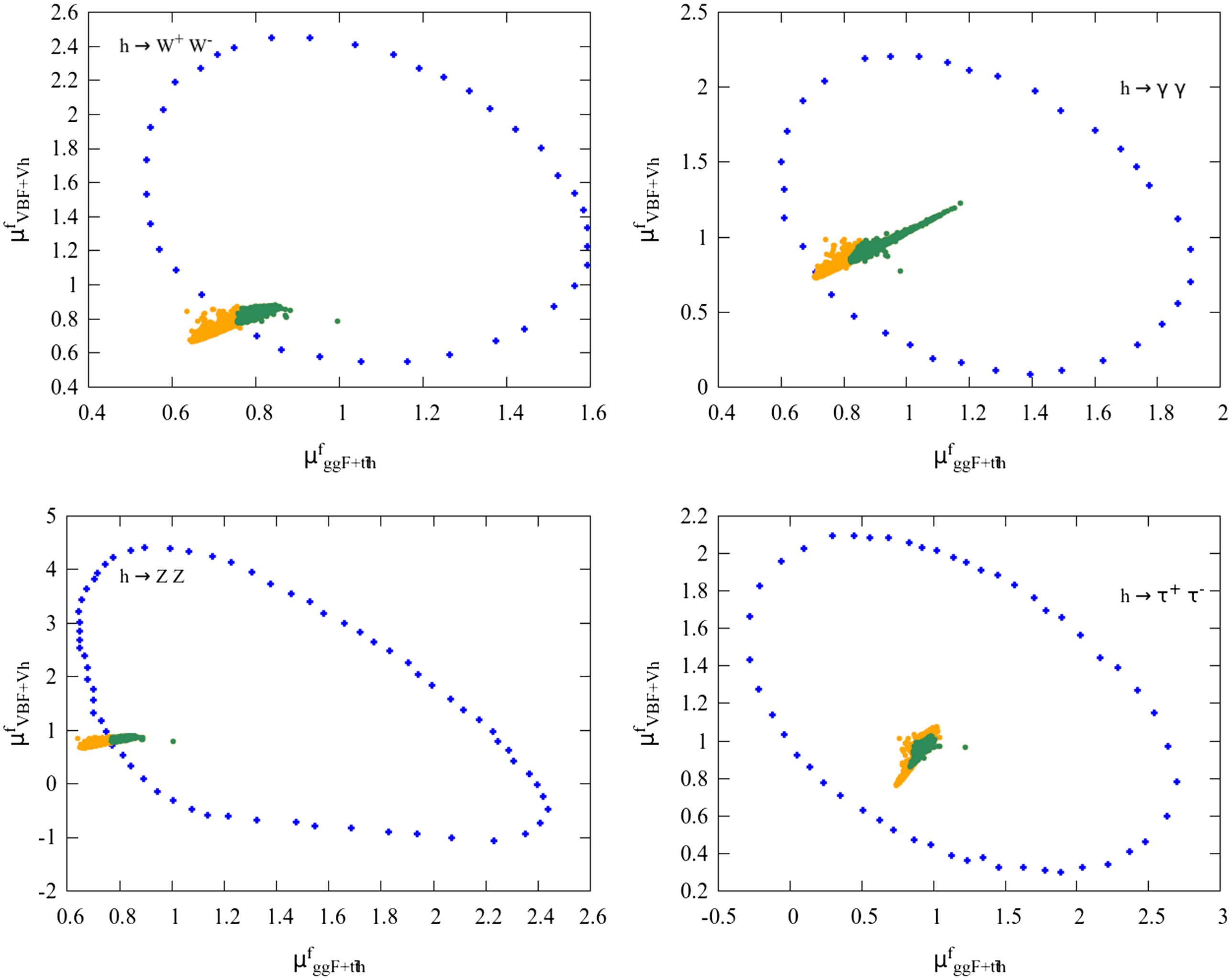

FIG. 10. The 95% C.L. contours in the $\mu^f_{ggF+t\bar{t}h} - \mu^f_{\mathrm{VBF+VH}}$ plane for Model-BWH.

[1] G. Aad *et al.* (ATLAS Collaboration), Phys. Lett. B **716**, 1 (2012).

[2] S. Chatrchyan *et al.* (CMS Collaboration), Phys. Lett. B **716**, 30 (2012).

[3] The ATLAS and CMS Collaborations, Report No. ATLAS-CONF-2015-044, http://cds.cern.ch/record/2052552.

[4] G. Aad *et al.* (ATLAS Collaboration), Eur. Phys. J. C **76**, 6 (2016).

[5] V. Khachatryan *et al.* (CMS Collaboration), Eur. Phys. J. C **75**, 212 (2015).

[6] For reviews on supersymmetry, see J. Wess and J. Bagger, *Supersymmetry and Supergravity*, 2nd ed. (Princeton University, Princeton, NJ, 1991); M. Drees, P. Roy, and R. M. Godbole, *Theory and Phenomenology of Sparticles* (World Scientific, Singapore, 2005); H. E. Haber and G. Kane, Phys. Rep. **117**, 75 (1985); H. P. Nilles, Phys. Rep. **110**, 1 (1984).

[7] S. P. Martin, Adv. Ser. Dir. High Energy Phys. **18**, 1 (1998).

[8] A. Djouadi, Phys. Rep. **459**, 1 (2008).

[9] CMS Public SUSY summary, https://twiki.cern.ch/twiki/pub/CMSPublic/SUSYSMSSummaryPlots8TeV/barplot_ICHEP2014.pdf.

[10] ATLAS Public SUSY summary, https://atlas.web.cern.ch/Atlas/GROUPS/PHYSICS/CombinedSummaryPlots/SUSY/ATLAS_SUSY_Summary/ATLAS_SUSY_Summary.png.

[11] G. Aad *et al.* (ATLAS Collaboration), Phys. Rev. Lett. **113**, 171801 (2014).

[12] V. Khachatryan *et al.* (CMS Collaboration), Phys. Lett. B **750**, 494 (2015).

[13] G. Aad *et al.* (ATLAS Collaboration), J. High Energy Phys. 01 (2016) 032.

[14] V. Khachatryan *et al.* (CMS Collaboration), J. High Energy Phys. 10 (2015) 144.

[15] G. Aad *et al.* (ATLAS Collaboration), Eur. Phys. J. C **76**, 45 (2016).
[16] G. Aad *et al.* (ATLAS Collaboration), Eur. Phys. J. C **75**, 412 (2015).
[17] V. Khachatryan *et al.* (CMS Collaboration), Phys. Lett. B **749**, 560 (2015).
[18] G. Aad *et al.* (ATLAS Collaboration), Phys. Rev. Lett. **114**, 081802 (2015).
[19] V. Khachatryan *et al.* (CMS Collaboration), Phys. Rev. D **94**, 052012 (2016).
[20] G. Aad *et al.* (ATLAS Collaboration), Phys. Rev. D **92**, 092004 (2015).
[21] G. Aad *et al.* (ATLAS Collaboration), Phys. Lett. B **744**, 163 (2015).
[22] V. Khachatryan *et al.* (CMS Collaboration), Phys. Lett. B **748**, 221 (2015).
[23] V. Khachatryan *et al.* (CMS Collaboration), J. High Energy Phys. 10 (2014) 160.
[24] G. Aad *et al.* (ATLAS Collaboration), J. High Energy Phys. 11 (2014) 056.
[25] V. Khachatryan *et al.* (CMS Collaboration), J. High Energy Phys. 12 (2015) 178.
[26] V. Khachatryan *et al.* (CMS Collaboration), J. High Energy Phys. 11 (2015) 018.
[27] V. Khachatryan *et al.* (CMS Collaboration), J. High Energy Phys. 12 (2015) 178.
[28] G. Aad *et al.* (ATLAS Collaboration), J. High Energy Phys. 03 (2015) 088.
[29] G. Aad *et al.* (ATLAS Collaboration), J. High Energy Phys. 03 (2016) 127.
[30] G. Aad *et al.* (ATLAS Collaboration), Eur. Phys. J. C **73**, 2465 (2013).
[31] M. Bisset, J. Li, and N. Kersting, arXiv:0709.1031.
[32] M. Bisset, J. Li, N. Kersting, R. Lu, F. Moortgat, and S. Moretti, J. High Energy Phys. 08 (2009) 037.
[33] A. Arhrib, R. Benbrik, M. Chabab, and C. H. Chen, Phys. Rev. D **84**, 115012 (2011).
[34] J. F. Gunion, H. E. Haber, M. Drees, D. Karatas, X. Tata, R. Godbole, and N. Tracas, Int. J. Mod. Phys. A **02**, 1035 (1987).
[35] J. F. Gunion and H. E. Haber, Nucl. Phys. **B307**, 445 (1988); **B402**, 569(E) (1993).
[36] A. Djouadi, P. Janot, J. Kalinowski, and P. M. Zerwas, Phys. Lett. B **376**, 220 (1996).
[37] G. Belanger, F. Boudjema, F. Donato, R. Godbole, and S. Rosier-Lees, Nucl. Phys. **B581**, 3 (2000).
[38] M. Bisset, M. Guchait, and S. Moretti, Eur. Phys. J. C **19**, 143 (2001).
[39] S. Y. Choi, M. Drees, J. S. Lee, and J. Song, Eur. Phys. J. C **25**, 307 (2002).
[40] C. Charlot, R. Salerno, and Y. Sirois, J. Phys. G **34**, N1 (2007).
[41] T. Li, Phys. Lett. B **728**, 77 (2014).
[42] G. Belanger, D. Ghosh, R. Godbole, and S. Kulkarni, J. High Energy Phys. 09 (2015) 214.
[43] B. Ananthanarayan, J. Lahiri, and P. N. Pandita, Phys. Rev. D **91**, 115025 (2015).
[44] A. Djouadi, L. Maiani, A. Polosa, J. Quevillon, and V. Riquer, J. High Energy Phys. 06 (2015) 168.
[45] R. Y. Zhang, W. G. Ma, L. H. Wan, and Y. Jiang, Phys. Rev. D **65**, 075018 (2002).
[46] T. Ibrahim, Phys. Rev. D **77**, 065028 (2008).
[47] S. Heinemeyer and C. Schappacher, Eur. Phys. J. C **75**, 230 (2015).
[48] ATLAS collaboration, Report Nos. ATL-PHYS-PUB-2009-079; ATL-COM-PHYS-2009-086.
[49] F. Moortgat, S. Abdullin, and D. Denegri, arXiv:hep-ph/0112046.
[50] A. Djouadi, J. L. Kneur, and G. Moultaka, Comput. Phys. Commun. **176**, 426 (2007).
[51] A. Djouadi, J. Kalinowski, and M. Spira, Comput. Phys. Commun. **108**, 56 (1998).
[52] Y. Amhis *et al.* (Heavy Flavor Averaging Group (HFAG) Collaboration), arXiv:1412.7515.
[53] G. Degrassi, S. Heinemeyer, W. Hollik, P. Slavich, and G. Weiglein, Eur. Phys. J. C **28**, 133 (2003); B. C. Allanach, A. Djouadi, J. L. Kneur, W. Porod, and P. Slavich, J. High Energy Phys. 09 (2004) 044; S. P. Martin, Phys. Rev. D **75**, 055005 (2007); R. V. Harlander, P. Kant, L. Mihaila, and M. Steinhauser, Phys. Rev. Lett. **100**, 191602 (2008); **101**, 039901(E) (2008); S. Heinemeyer, O. Stal, and G. Weiglein, Phys. Lett. B **710**, 201 (2012); A. Arbey, M. Battaglia, A. Djouadi, and F. Mahmoudi, J. High Energy Phys. 09 (2012) 107.
[54] A. Djouadi, M. M. Muhlleitner, and M. Spira, Acta Phys. Pol. B **38**, 635 (2007).
[55] G. Belanger, F. Boudjema, A. Pukhov, and A. Semenov, Comput. Phys. Commun. **185**, 960 (2014).
[56] LEP Higgs Working Group for Higgs boson searches and ALEPH and DELPHI and L3 and OPAL Collaborations, arXiv:hep-ex/0107031.
[57] M. Aaboud *et al.* (ATLAS Collaboration), J. High Energy Phys. 09 (2016) 001.
[58] V. Khachatryan *et al.* (CMS Collaboration), Phys. Rev. Lett. **117**, 051802 (2016).
[59] J. F. Gunion and H. E. Haber, Phys. Rev. D **67**, 075019 (2003).
[60] B. Bhattacherjee, A. Chakraborty, and A. Choudhury, Phys. Rev. D **92**, 093007 (2015).
[61] ATLAS collaboration, Report No. ATLAS-CONF-2016-021, http://cds.cern.ch/record/2147445.
[62] ATLAS collaboration, Report No. ATLAS-CONF-2016-016, http://cds.cern.ch/record/2141005.
[63] B. Bhattacherjee and A. Choudhury, Phys. Rev. D **91**, 073015 (2015).
[64] CMS Collaboration, Report No. CMS-PAS-HIG-16-006, http://cds.cern.ch/record/2160252.
[65] ATLAS collaboration, Report No. ATLAS-CONF-2015-061, http://cds.cern.ch/record/2114827.
[66] ATLAS collaboration, Report No. ATLAS-CONF-2016-015, http://cds.cern.ch/record/2141003.
[67] M. Aaboud *et al.* (ATLAS Collaboration), Phys. Lett. B **759**, 555 (2016).
[68] G. Aad *et al.* (ATLAS Collaboration), J. High Energy Phys. 04 (2014) 169.
[69] G. Aad *et al.* (ATLAS Collaboration), J. High Energy Phys. 05 (2014) 071.
[70] G. Aad *et al.* (ATLAS Collaboration), J. High Energy Phys. 10 (2014) 096.

[71] G. Aad *et al.* (ATLAS Collaboration), Eur. Phys. J. C **75**, 208 (2015).

[72] G. Aad *et al.* (ATLAS Collaboration), Phys. Rev. D **93**, 052002 (2016).

[73] V. Khachatryan *et al.* (CMS Collaboration), Phys. Rev. D **90**, 092007 (2014).

[74] V. Khachatryan *et al.* (CMS Collaboration), Eur. Phys. J. C **74**, 3036 (2014).

[75] M. Chakraborti, U. Chattopadhyay, A. Choudhury, A. Datta, and S. Poddar, J. High Energy Phys. 11 (2015) 050.

[76] A. Choudhury and S. Mondal, Phys. Rev. D **94**, 055024 (2016).

[77] W. Beenakker, R. Hopker, and M. Spira, arXiv:hep-ph/9611232.

[78] http://www.iacs.res.in/conferences/lhcdm2015/SwB_IACS_Feb2014.pdf.

[79] J. Alwall, R. Frederix, S. Frixione, V. Hirschi, F. Maltoni, O. Mattelaer, H.-S. Shao, T. Stelzer, P. Torrielli, and M. Zaro, J. High Energy Phys. 07 (2014) 079.

[80] T. Sjostrand, S. Mrenna, and P. Z. Skands, J. High Energy Phys. 05 (2006) 026.

[81] R. V. Harlander, S. Liebler, and H. Mantler, Comput. Phys. Commun. **184**, 1605 (2013); R. V. Harlander and W. B. Kilgore, Phys. Rev. Lett. **88**, 201801 (2002); Phys. Rev. D **68**, 013001 (2003); U. Aglietti, R. Bonciani, G. Degrassi, and A. Vicini, Phys. Lett. B **595**, 432 (2004); G. Degrassi and P. Slavich, J. High Energy Phys. 11 (2010) 044; G. Degrassi, S. Di Vita, and P. Slavich, J. High Energy Phys. 08 (2011) 128; R. Harlander and P. Kant, J. High Energy Phys. 12 (2005) 015.

[82] J. de Favereau, C. Delaere, P. Demin, A. Giammanco, V. Lemaître, A. Mertens, and M. Selvaggi (DELPHES 3 Collaboration), J. High Energy Phys. 02 (2014) 057.

[83] G. Aad *et al.* (ATLAS Collaboration), Phys. Rev. D **90**, 012004 (2014).

[84] ATLAS collaboration, Report No. ATLAS-CONF-2014-017, https://cds.cern.ch/record/1692660.

[85] ATLAS Collaboration, Report No. ATL-PHYS-PUB-2014-010, https://cds.cern.ch/record/1735031.